

Investigation of Carotid Atherosclerosis Ultrasound Image Using Computational Hemodynamics

by

Dabasish Kumar Saha

A thesis submitted in partial fulfillment of the requirements for the degree of Master of
Science in Electronics and Communication Engineering



Khulna University of Engineering & Technology

Khulna 9203, Bangladesh

February 2016

Declaration

This is to certify that the thesis work entitled “*Investigation of Carotid Atherosclerosis Ultrasound Image Using Computational Hemodynamics*” has been carried out by *Dabasish Kumar Saha* in the Department of *Electronics and Communication Engineering*, Khulna University of Engineering & Technology, Khulna, Bangladesh. The above thesis work or any part of this work has not been submitted anywhere for the award of any degree or diploma.

Signature of Supervisor

Signature of Candidate

Approval

This is to certify that the thesis work submitted by *Dabasish Kumar Saha* entitled “*Investigation of Carotid Atherosclerosis Ultrasound Image Using Computational Hemodynamics*” has been approved by the board of examiners for the partial fulfillment of the requirements for the degree of *Master of Science* in the Department of *Electronics and Communication Engineering (M.Sc. Eng. in ECE)*, Khulna University of Engineering & Technology, Khulna, Bangladesh in February 2016.

BOARD OF EXAMINERS

1. _____ Chairman
Dr. A. B. M. Aowlad Hossain (Supervisor)
Professor
Khulna University of Engineering & Technology (KUET)
Khulna, Bangladesh.
2. _____ Member
Dr. Md. Mostafizur Rahman
Professor and Head of the Department
Department of Electronics and Communication Engineering
Khulna University of Engineering & Technology (KUET)
Khulna, Bangladesh.
3. _____ Member
Dr. Md. Osman Goni
Professor
Khulna University of Engineering & Technology (KUET)
Khulna, Bangladesh.
4. _____ Member
Dr. Md. Foisal Hossain
Associate Professor
Khulna University of Engineering & Technology (KUET)
Khulna, Bangladesh.
5. _____ Member
Dr. Md. Maniruzzaman (External)
Professor
Khulna University
Khulna, Bangladesh.

Dedicated to My Parents

Acknowledgement

First of all, I am thanking and expressing my immense gratefulness to the almighty for his kindness and grace to me for the successful completion of my thesis work. Then I would like to express my deep appreciation and profound respect to my supervisor, **Dr. A. B. M. Aowlad Hossain**, Professor, Department of Electronics and Communication Engineering (ECE), Khulna University of Engineering & Technology (KUET), Bangladesh, for his invaluable advices, ardent initiatives, scholastic guidance, constant and continuous inspiration, constructive suggestions and kind cooperation throughout the entire progress of this thesis work titled as **“Investigation of Carotid Atherosclerosis Ultrasound Image Using Computational Hemodynamics”**. Especially, our meetings during the last couple of months were of great support. He sacrificed his enough valuable time for supporting me. I am also so much grateful to my supervisor for his loving and cordial advices to prepare my thesis proposal in the beginning of this thesis work and my final thesis paper. The systematic and articulate approach of my supervisor in analyzing a problem, his persistent enthusiasm and overall presence will be always recalled by me in all of my future activities.

Then I would take this opportunity to express my deepest appreciation to **Prof. Dr. Md. Mostafizur Rahman**, Head of the department of ECE, KUET, for providing departmental facilities.

Then I would like to acknowledge my deep gratitude to my graduation committee.

Finally, I wish to complement all the concerned teachers/alumni of the department and friends who have directly or indirectly helped at different stages of the research work.

February 2016

Dabasish Kumar Saha

Abstract

Brain stroke is a major cause of mortality and disability in recent decades. Carotid atherosclerosis is considered an important contributor to the growing problem of brain stroke. Carotid atherosclerosis resulted from an accumulation of fat, cholesterol, Calcium, and other materials in arterial walls that create complex hemodynamics. Furthermore, elevated blood viscosity is associated with atherosclerosis and its growth. Hence, increased blood viscosity is also an independent risk factor for atherosclerotic diseases. Though conventional ultrasound techniques used for flow estimation due to the real time scanning capability, still there are scopes to enhance the image quality. Moreover, atherosclerosis related viscosity changes effects are not considered in conventional techniques. The knowledge of the carotid artery hemodynamics resulted due to atherosclerosis with different level of blood viscosity can provide more information on artery stenosis and symptoms, and the risk of stroke. Therefore, improvement in flow imaging has great clinical importance to understand the origin and evolution of disease. Investigation and detection of viscosity change and its effect might be helpful for better diagnosis of carotid atherosclerosis, which is a major emphasis of this thesis. In this simulation work, hemo-disturbances have been investigated in realistic normal and atherosclerotic carotid using finite element method (FEM) based computational fluid dynamics (CFD) under different viscosities consideration. The computed data has been used to simulate color flow image of blood velocities using ultrasound radio frequency (RF) signals to considering ultrasound potentiality in atherosclerosis diagnosis. The ultrasound simulated flow characteristics have been compared with FEM computed flow behavior and found a good agreement between them. It has been observed that the blood velocities increase noticeably in carotid atherosclerotic growths whereas velocities are almost uniform in the normal carotid. The severity stages of the models have been examined quantitatively. It is also found that viscosity induced contrast is not negligible and importantly, it is detectable from multiple steps ultrasound flow images. The findings of this study suggest that ultrasound based blood flow image can detect the viscosity change effect related to atherosclerosis growth. So, incorporation of the viscosity changes contrast can enhance the quality of ultrasound flow image. It is expected that the outcomes of this thesis work might be useful to diagnosis the present conditions and predict the future progressions of carotid atherosclerosis to minimize the risk of stroke.

Contents

	PAGE
Title page	i
Declaration	ii
Approval	iii
Acknowledgement	v
Abstract	vi
Contents	vii
List of Tables	x
List of Figures	xi
List of Abbreviation	xiii
CHAPTER I: Introduction	1-6
1.1 Introduction	2
1.2 Background Information	2
1.3 Motivation	4
1.4 Challenges	5
1.5 Objectives	6
1.6 Thesis Outline	6
CHAPTER II: Introduction to Carotid Atherosclerosis	7-17
2.1 Introduction	8
2.2 Human Circulatory System	8
2.3 Basics of Carotid Atherosclerosis	9
2.4 Causes and Promotion of Atherosclerosis	11
2.5 Relationship between Viscosity and Carotid Atherosclerosis	16
2.6 Summary	17

CHAPTER III: Basics of Hemodynamics	18-27
3.1 Introduction	19
3.2 Definition of Hemodynamics	19
3.3 Types of Blood Flow	20
3.4 Blood Flow Physics	22
3.5 Computational Fluid Dynamics (CFD)	23
3.6 Finite Element Method	25
3.7 Summary	27
CHAPTER IV: Basics of Ultrasound Flow Imaging	28-44
4.1 Introduction	29
4.2 Evolution of Ultrasound Imaging	29
4.3 Generation of Ultrasound Pulses	30
4.4 Ultrasound Wavelength and Frequency	30
4.5 Measurement of Flow Signals	33
4.6 Simulation of Flow Imaging System	36
4.7 Velocity Estimation Using Doppler Method	37
4.8 Velocity Estimation Using Autocorrelation Algorithm	40
4.9 Color Flow Mapping Using Cross Correlation	42
4.10 Summary	44
CHAPTER V: Simulation Methodology	45-62
5.1 Introduction	46
5.2 Simulation Strategy	46
5.3 Simulation of Blood Flow Using CFD	48
5.3.1 Carotid Artery Geometry Model	49
5.3.2 Material Properties for Flow Model	50
5.3.3 Discretization of the Geometrical Model	51
5.4 Ultrasound Signal Simulation for Flow Imaging	52
5.4.1 The Spatial Impulse Response Concept in Field II	53
5.4.2 Transducer	53

5.4.3 Sound Beam Formation	55
5.4.4 Focusing	56
5.4.5 Ultrasound Beam Simulation	57
5.4.6 Ultrasound Color Flow Image (CFI) Simulation	59
5.5 Summary	62
CHAPTER VI: Result Analysis and Discussions	63-71
6.1 Introduction	64
6.2 Analysis of CFD Simulated Images	64
6.3 Analysis of Ultrasound Based Simulated Images	66
6.4 Investigation on Viscosity Change Tracking Capability of Ultrasound Scanning	68
6.5 Discussions	70
CHAPTER VII: Conclusions	72-75
7.1 Outcomes	73
7.2 Contributions in this Research	74
7.3 Limitations and Future Perspectives	74
References	76
List of Publication	83

LIST OF TABLES

Table No.	Description	Page
2.1	Progression of atherosclerosis	15
2.2	Comparison of IMT between healthy patients and atherosclerotic patients	15
2.3	Definition of stenosis level	15
2.4	Variation of blood velocity due to different stenosis	16
5.1	Measurement of Reynolds numbers for three different blood viscosities	51
6.1	Variation of blood velocity due to different stenosis	70

LIST OF FIGURES

Figure No.	Description	Page
2.1	Blood circulation system	9
2.2	A shows the location of the right carotid artery in the head and neck. B shows the inside of a normal carotid artery that has normal blood flow. C shows the inside of a carotid artery that has plaque buildup and reduced blood flow.	10
2.3	Endothelial Dysfunction in Atherosclerosis	12
2.4	Fatty-Streak Formation in Atherosclerosis	13
2.5	Formation of an Advanced Complicated Lesion of Atherosclerosis	13
2.6	Unstable Fibrous Plaques in Atherosclerosis	14
3.1	Process of Computational Fluid Dynamics	25
4.1	Attenuation of ultrasound waves and its relationship to wave frequency	31
4.2	A comparison of the resolution and penetration of different ultrasound transducer frequencies	31
4.3	Schematic representation of ultrasound pulse generation	32
4.4	Degrees of attenuation of ultrasound beams as a function of the wave frequency in different body tissues	32
4.5	Coordinate system for finding the movement of blood particles	33
4.6	RF sampling of simulated signal from blood vessel	35
4.7	Demodulation schemes for obtaining a complex signal for determining the sign of the velocity	36
4.8	Example of autocorrelation velocity estimate	41
4.9	Principle of velocity estimation using cross-correlation	42
4.10	Example of cross-correlation velocity estimate	43

5.1	Flow chart of simulation strategy	47
5.2	Carotid artery bifurcation	49
5.3	Carotid artery model for different cases	50
5.4	Mesh diagram of the normal and stenosed carotid artery model	52
5.5	Piezoelectric & reverse piezoelectric effect	54
5.6	Rectangles for a 16 elements linear array transducer	55
5.7	Ultrasound focusing concept	56
5.8	Different array of transducer	57
5.9	Ultrasound beam pattern crosssection	58
5.10	Received response for the individual elements and the summed signal for one line	58
5.11	Simulated ultrasound RF signals and B-mode image for three effective points scatterers with different echogeneities	59
6.1	Parabolic velocity profile for inlet boundary condition	64
6.2	(a) Stenosed carotid artery model with bifurcation and (b) computed velocity image	65
6.3	CFD simulation images for viscosities of (a) 3.5mPa-s, (b) 7mPa-s and (c) 10mPa-s	66
6.4	Comparison of CFD computed and ultrasound simulated color flow velocity image for different blood flow models	67
6.5	(a) Contour plot and (b) vector plot of velocity distribution for abnormal model-1	68
6.6	Comparison of CFD and ultrasound images considering viscosity changes	69

List of Abbreviation

Autocorrelation Method	AM
Color Flow Imaging	CFI
Color Flow Mapping	CFM
Common Carotid Artery	CCA
Computational Fluid Dynamics	CFD
Computer Aided Design	CAD
Continuous Wave	CW
Degree of Freedom	DOF
Endothelial Cell	EC
External Carotid Artery	ECA
Finite Element Analysis	FEA
Finite Element Method	FEM
High Density Lipoprotein	HDL
Internal Carotid Artery	ICA
Intima Media Thickness	IMT
Low Density Lipoprotein	LDL
Partial Differential Equation	PDE
Pulse Repetition Frequency	PRF
Pulsed Wave	PW
Radio Frequency	RF
Red Blood Cell	RBC
Region of Interest	ROI
Smooth Muscle Cell	SMC
Ultrasound	US
White Blood Cell	WBC

CHAPTER I

Introduction

Chapter Outlines

- ❖ Introduction
- ❖ Background Information
- ❖ Motivation
- ❖ Challenges
- ❖ Objectives
- ❖ Thesis Outline

CHAPTER I

Introduction

1.1 Introduction

The number of stroke deaths is expected to increase from 5.7 million in 2005 to 7.8 million in 2030 according to the comprehensive World Health Organization data which contains information on the vast majority (72%) of the world's population. Mortality rates increasing from 89 to 98 per 100,000 over the same period due to the aging population, poor diet, physical inactivity and tobacco use [1]. Atherosclerosis – a degenerative, progressive disease characterized by the formation of atheroma or plaques composed of lipid accumulation, inflammatory cells and fibrous elements in the carotid artery – is considered the “single most important contributor to the growing burden of stroke” [2]. Stroke is the third highest cause of death in the USA, behind heart disease and cancer, and places a huge cost on the health care system with an estimate of \$74billion in 2010 [3]. Stroke related diseases have become increasingly widespread in Bangladesh also [4]. Gaining a better understanding of the causes of stroke has the potential to save lives and significantly reduce the burden on the health care system. A noninvasive way of monitoring the cardiovascular blood flow velocity will help clinicians assessing the cardiovascular system and that could prevent imminent stroke. Ultrasound based blood flow imaging might be a promising methods to investigate the condition of arteries due to its real time scanning capability, low cost and ubiquitousness.

1.2 Background Information

The cardiovascular diseases represent risks to the human health and its pathologies can lead to the death of the patient. The early diagnostic of these pathologies is important to avoid clinical cases such as atherosclerosis, aneurysm, thrombosis etc. In fact, the cardiovascular diseases harm the heart and vascular system functions increasing the risk of heart attacks and brain stroke. One of the main cardiovascular diseases is the atherosclerosis, which results from an accumulation of lipids and other materials in arterial walls, and can cause a focal luminal narrowing as well as loss of elasticity in the arteries. This disease often leads to heart attack and brain stroke, leading causes of death in the industrial world [5]-[7]. Atherosclerosis

appears to preferentially originate in disturbed flow fields. Efficient imaging of these disturbed flow fields may help in improving preliminary diagnosis of arterial disease, as well as contribute to the understanding of the origin and progression of cardiovascular disease.

Blood viscosity is the thickness and stickiness of blood. It is a direct measure of the ability of blood to flow through the vessels. It is the critical biophysical parameter that determines how much friction the blood causes against the vessels; how hard the heart has to work to pump blood; and how much oxygen is delivered to organs and tissues. Whole blood is a non-Newtonian fluid, and its viscosity changes with its velocity. It is noticeable that blood at diastole usually 5 to 20 times as viscous as the same blood at systole [8]. Blood viscosity is an important factor, which is related to the atherosclerosis. Recent studies show that, blood viscosity is increased in men with carotid atherosclerosis. Blood viscosity is important because high blood viscosity creates low shear stress where the fatty deposits occur. This means that in between heart beats the blood thickens and swirls around, causing eddies and turbulence. Turbulent blood flow progressively damages the cells that line the arteries. As a result plaque tends to deposit most heavily in the low shear regions of the arteries where atherosclerosis grows up. This result blood flow is further impeded, leading to more turbulence and more plaque deposition. When the plaque deposition reaches a critical stage, it becomes a major cause of cardiovascular diseases such as heart attacks and stroke [9]. Blood viscosity also affects blood pressure. Elevated blood pressure is a major risk factor for developing atherosclerosis and becomes a stronger risk factor after age 45 [10]. Elevated blood viscosity increases peripheral resistance. Blood pressure must increase to maintain cardiac output when there increased resistance due to hyper-viscous blood. Increased blood pressure then damages arteries further and increases the risk of stroke and heart attack. The effects of blood viscosity, taken together with an understanding of the dynamics of blood flow in artery, explain why it is that atherosclerotic plaques are found only in specific locations in the body.

Carotid artery atherosclerosis and its relationship to stroke have clinically been an area of considerable research focus due to the devastating effects of artery to artery emboli and the potential for diagnostic and therapeutic advances. Indeed, the accessibility beneath the skin of the neck of this source of stroke to noninvasive study has allowed the opportunity for far greater understanding of the pathophysiology of stroke disease processes.

Ultrasound techniques have gained widespread applications in clinical diagnosis for its low cost, fast scan and portable facilities. Ultrasonic imaging techniques are the subject of intense research activity and the capabilities of new approaches to provide novel information of considerable actual and potential clinical value are highly attractive. In traditional ultrasonic imaging, the signals which form the image are basically owing to reflection and scattering of ultrasound where there are differences in the characteristic impedances of the media being imaged. Medical ultrasound scanners can be used for both displaying gray-scale images of the anatomy and for visualizing the blood flow dynamically in the body. The systems can interrogate the flow at a single position in the body and there find the velocity distribution over time. Color Doppler ultrasound is inexpensive, widely accessible, fast and safe, and provides real-time images of endovascular structure; also measuring techniques have improved to provide accurate information on the flow fields. Today's ultrafast ultrasound blood imaging technique provides more intuitive and characteristic representation of flow and also gives better quantification of fast transitory cardiac events.

1.3 Motivation

From the information given in the previous section it can be concluded that, stroke are most often caused by carotid artery atherosclerosis that creates hemo-disturbances. As the disease progresses the visco-elastic properties of the artery wall also changes. The knowledge of carotid hemodynamics resulted due to atherosclerosis can clarify the relationship between artery stenosis that create disturb flow fields and symptoms, and, finally, the risk of stroke.

Carotid atherosclerosis can therefore be diagnosed from the information of blood flow disturbance (hemodynamics). Hence efficient imaging of this disturbed flow field can help us in diagnosing arterial disease in an early stage and give us proper direction to understanding of atherosclerosis and progression of this cardiovascular disease. In several studies, researcher suggested blood flow model using the fluid dynamics concept to analyze the mechanical behavior of the blood vessels. These models are useful to investigate the vessels condition and flow information using image or measurement data directly or inversely [11]-[15]. Some studies used the CFD data to construct the ultrasound based velocity images using pulsed-wave (PW) Doppler technique or color flow imaging (CFI) for blood flow analysis [16]. But, still there are scopes to improve the image quality of the flow which is important for effective

diagnosis of atherosclerosis. Furthermore, incorporation of blood viscosity related information can enhance the quality of ultrasound based blood velocity images. As, elevated blood viscosity is associated with atherosclerosis and its growth, the knowledge of the arterial hemodynamics resulted due to atherosclerosis with different levels of blood viscosity can elucidate the relationship between artery stenosis and symptoms, and, finally, the risk of stroke. So we can introduce viscosity related information for better understanding about the condition of artery.

1.4 Challenges

In this work, we have focused on carotid arteries due to the complexity of the local flow field, their susceptibility to atherosclerosis, and because the location is easily accessible with ultrasound. Direct investigation requires physical subjects and instruments with raw data accessing facilities, which are very difficult, bigger and lengthy tasks. Simulation study with realistic consideration is a possible and comfy alternative, which are a common practice in such cases.

Computational fluid dynamics (CFD) models have become very effective tools for predicting the flow field within the vessels, and for proper understanding the relationship between local hemodynamics, and the initiation and progression of vascular wall pathologies. Realistic flow fields can be obtained with computational fluid dynamics (CFD), which solves the non-linear equations for conservation of mass and momentum in a discretized form. Modeling a proper realistic flow field is very difficult. Therefore, effective modeling and rigorous analysis is challenging to obtain a better understanding of diagnostic and functional aspects of the blood flow.

In ultrasound color flow imaging (CFI), different correlation algorithm such as auto or cross-correlation is used for velocity measurement. An efficient correlation algorithm is very demanding for developing a better quality ultrasound velocity image to accurately understand the progression of diseases. As speckle noise is very common in ultrasound signals effective filtering is also necessary. Therefore, reconstruction and post-processing tasks for a better quality ultrasound velocity image is also challenging.

1.5 Objectives

The main objective of this thesis was to investigate carotid atherosclerosis ultrasound images using computational model of blood flow through carotid artery. Since various factors have to be considered for effective analysis, the objective divided into following step-by-step approaches:

- i) Effective modeling of the realistic carotid artery with the stenosis to mimic atherosclerosis as described before.
- ii) Simulation of blood flow using computational hemodynamics and compute displacement data under realistic boundary constraints.
- iii) Generation of ultrasound RF signals using the data obtained from computational hemodynamics through finite element analysis.
- iv) Ultrasound blood flow image simulation using simulated RF signals.
- v) Investigation of obtained images in qualitative and quantitative way.

1.6 Thesis Outline

Chapter 2 describes a basic knowledge about carotid atherosclerosis and its growth and its relation to blood viscosity.

Chapter 3 contains a basic knowledge about hemodynamics and computational Fluid dynamics, how it can be applied in more accurate blood flow modeling, finite element method (FEM) and different types of blood flow.

Chapter 4 presents a brief introduction on ultrasound imaging and a details discussion on ultrasound based flow estimation techniques.

Chapter 5 describes the methodology used in this simulation study. Both CFD based simulation method and ultrasound based simulation method for computing blood flow images are explained rigorously in this chapter.

Chapter 6 presents an analysis on the resultant simulation images, their comparison, and a discussion on the obtained results accordingly.

Chapter 7 mentions some of the important findings, limitations and future possibilities of this work.

CHAPTER II

Introduction to Carotid Atherosclerosis

Chapter Outlines

- ❖ Introduction
- ❖ Human Circulatory System
- ❖ Basics of Carotid Atherosclerosis
- ❖ Causes and Promotion of Atherosclerosis
- ❖ Relationship between Viscosity and Carotid Atherosclerosis
- ❖ Summary

CHAPTER II

Introduction to Carotid Atherosclerosis

2.1 Introduction

Carotid artery atherosclerosis is a particular presentation of the larger systemic disease of atherosclerosis which affects many organs. Carotid atherosclerosis is a major public health problem, which is expected to increase in future years as our population ages at an accelerated pace. This chapter examines the relationship between the structural stability of carotid atherosclerotic plaque forming at the bifurcation of the common, internal/external carotids and the symptomatology of such lesions. The theory behind the formation of carotid atherosclerosis in human body and its growth is then described. Finally, the relationship between blood viscosity and carotid atherosclerosis and its growth is discussed.

2.2 Human Circularity System

Human circularity system is responsible for carrying oxygen and nourishment to organs and disposing the waste products resulting from metabolism. Figure 2.1 shows the human blood circulation system. It consists of:

-) Heart: Which is responsible for pumping action of blood into aorta.
-) Blood: which is made of two parts:
 - Plasma: which makes up 55 percent of blood volume.
 - Formed cellular elements (red and white blood cells, and platelets) which combine to make the remaining 45 percent of blood volume.
-) Blood vessels: The blood vessels are the part of the cardiovascular system that transports blood throughout the body. There are three major types of blood vessels
 - Arteries: the function of the arteries is to transport blood under high pressure to the tissues, therefore, the arteries have strong vascular walls, and blood flows at a high velocity in the arteries.
 - Capillaries: which enable the actual exchange of water and chemicals between the blood and the tissues. To have this role, the capillary walls are very thin.

- Veins: which carry blood from the capillaries back toward the heart, they are a major reservoir of extra blood. The pressure in the venous system is very low, therefore venous walls are thin.

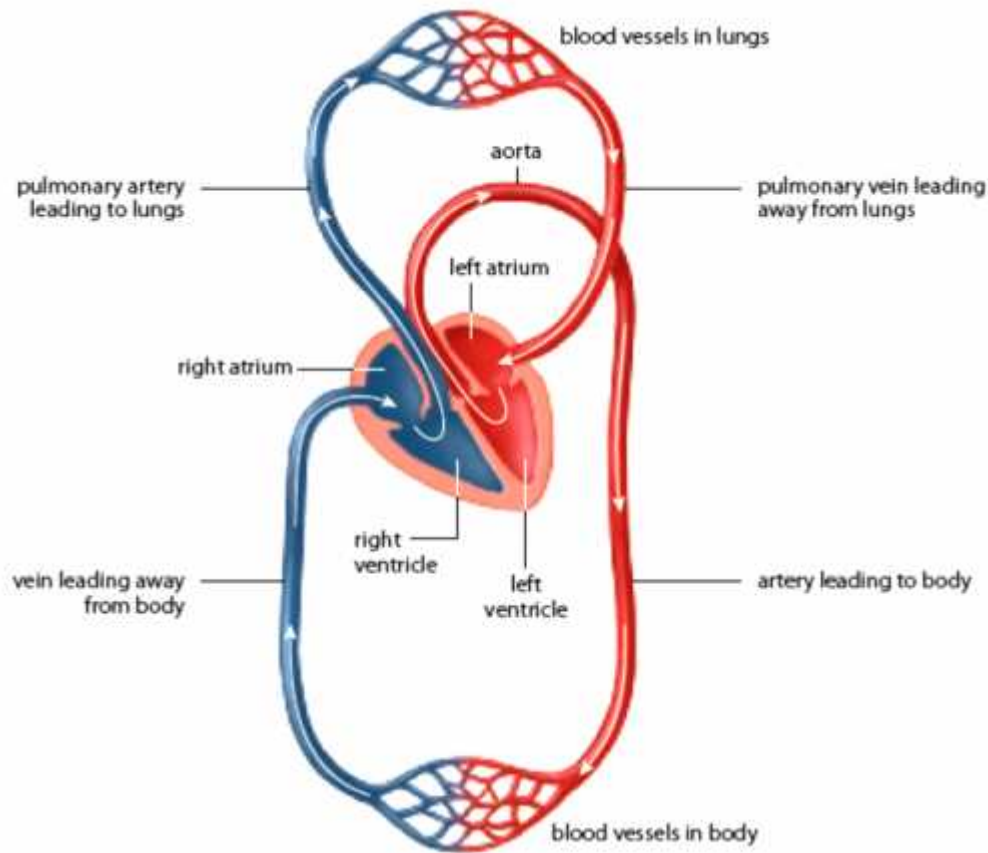


Figure 2.1 Blood circulation system [17].

2.3 Basics of Carotid Atherosclerosis

Atherosclerosis is an inflammatory disease in which plaque builds up inside our arteries. Arteries are blood vessels that carry oxygen-rich blood to our heart and other parts of our body. Atherosclerotic plaques are consisting of necrotic cores, calcified regions, accumulated modified lipids, inflamed smooth muscle cells (SMCs), endothelial cells (ECs), leukocytes, and foam cells [18]. These features of atherosclerotic plaques illustrate that atherosclerosis is a complex disease, and many components of the vascular, metabolic, and immune systems are involved in this process. Although low-density lipoprotein (LDL) remains the most important risk factor for atherosclerosis, immune and inflammatory mechanisms of atherosclerosis have

gained tremendous interest in the past 20 years [18]-[20]. Over time, plaque hardens and narrows our arteries. This limits the flow of oxygen-rich blood to our organs and other parts of our body. The lesions of atherosclerosis occur principally in large and medium-sized elastic and muscular arteries and can lead to ischemia of the heart, brain, or extremities, resulting in infarction. They may be present throughout a person's lifetime. In fact, the earliest type of lesion, the so-called fatty streak, which is common in infants and young children, [21] is a pure inflammatory lesion, consisting only of monocyte-derived macrophages and lymphocytes [22]. In persons with hypercholesterolemia, the influx of these cells is preceded by the extracellular deposition of amorphous and membranous lipids [21], [23].

There are two common carotid arteries, one on each side of our neck. They each divide into internal and external carotid arteries. The internal carotid arteries supply oxygen-rich blood to our brain. The external carotid arteries supply oxygen-rich blood to our face, scalp, and neck. Carotid atherosclerosis is serious because it can cause a stroke, also called a "brain stroke." A stroke occurs if blood flow to our brain is cut off. If blood flow is cut off for more than a few minutes, the cells in our brain start to die. This impairs the parts of the body that the brain cells control. A stroke can cause lasting brain damage; long-term disability, such as vision or speech problems or paralysis (an inability to move); or death [24].

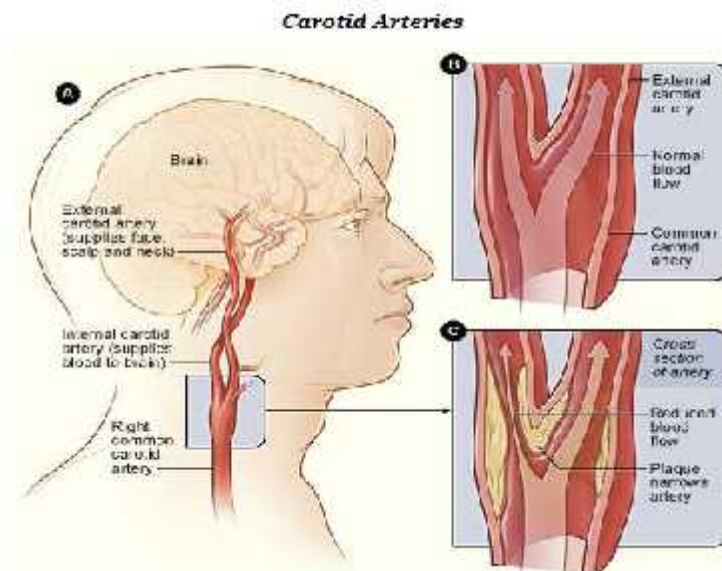


Figure 2.2 **A** shows the location of the right carotid artery in the head and neck, **B** shows the inside of a normal carotid artery that has normal blood flow, and **C** shows the inside of a carotid artery that has plaque buildup and reduced blood flow [18].

2.4 Causes and Promotion of Atherosclerosis

Numerous pathophysiologic observations in humans and animals led to the formulation of the response-to-injury hypothesis of atherosclerosis, which initially proposed that endothelial denudation was the first step in atherosclerosis [25]. The most recent version of this hypothesis emphasizes endothelial dysfunction rather than denudation. Whichever process is at work, each characteristic lesion of atherosclerosis represents a different stage in a chronic inflammatory process in the artery. If this characteristic lesion of atherosclerosis is unabated and excessive, this process will result in an advanced, complicated lesion. Possible causes of endothelial dysfunction leading to atherosclerosis include elevated and modified LDL. This elevated and modified LDL is caused by cigarette smoking, hypertension, and diabetes mellitus; genetic alterations; elevated plasma homocysteine concentrations; infectious microorganisms such as herpesviruses or *Chlamydia pneumoniae*; and combinations of these or other factors. Regardless of the cause of endothelial dysfunction, atherosclerosis is a highly characteristic response of particular arteries [25]-[29]. The endothelial dysfunction that results from the injury leads to compensatory responses that alter the normal homeostatic properties of the endothelium. Thus, the different forms of injury increase the adhesiveness of the endothelium with respect to leukocytes or platelets, as well as its permeability. The injury also induces the endothelium to have procoagulant instead of anticoagulant properties and to form vasoactive molecules, cytokines, and growth factors. If the inflammatory response does not effectively neutralize or remove the offending agents, it can continue indefinitely. In doing so, the inflammatory response stimulates migration and proliferation of smooth-muscle cells that become intermixed with the area of inflammation to form an intermediate lesion. If these responses continue unabated, they can thicken the artery wall. This compensates by gradual dilation, so that up to a point, the lumen remains unaltered, [30] a phenomenon termed “remodeling.” As for the inflammatory cells, granulocytes are rarely present during any phase of atherogenesis [31]. Instead, the response is mediated by monocyte-derived macrophages and specific subtypes of T lymphocytes at every stage of the disease [32], [33]. Continued inflammation results in increased numbers of macrophages and lymphocytes, which both emigrate from the blood and multiply within the lesion. Activation of these cells leads to the release of hydrolytic enzymes, cytokines, chemokines, and growth factors [34], [35]. This can induce further damage and eventually lead to focal necrosis [36]. Thus, cycles of accumulation

of mononuclear cells, migration and proliferation of smooth-muscle cells and formation of fibrous tissue lead to further enlargement and restructuring of the lesion, so that it becomes covered by a fibrous cap. This overlies a core of lipid and necrotic tissue, a so-called advanced, complicated lesion. At some point, the artery can no longer compensate by dilation. This point the lesion may then intrude into the lumen and alter the flow of blood.

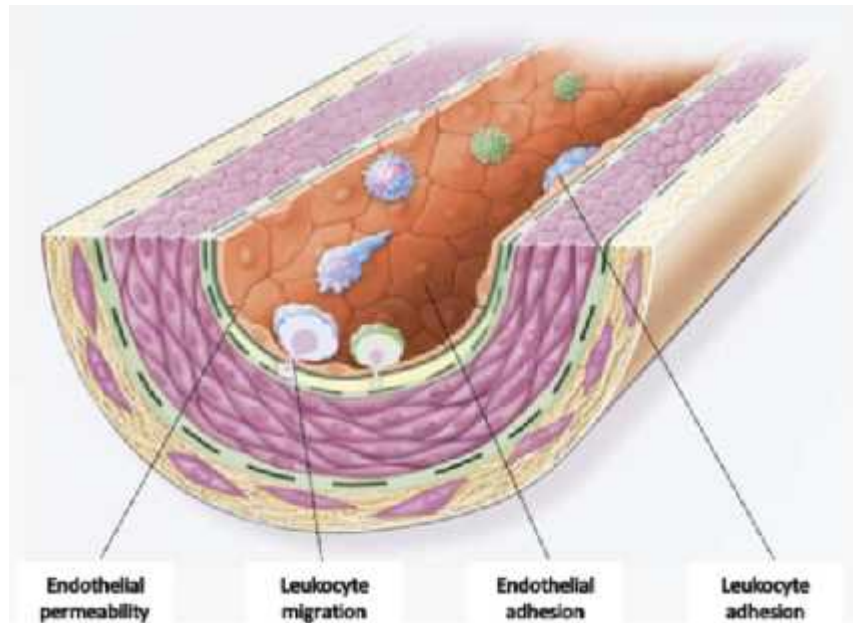


Figure 2.3 Endothelial Dysfunction in Atherosclerosis [18].

The earliest changes that precede the formation of lesions of atherosclerosis take place in the endothelium that shown in Fig. 2.3. These changes include increased endothelial permeability to lipoproteins and other plasma constituents. This are mediated by nitric oxide, prostacyclin, platelet-derived growth factor, angiotensin II, and endothelin. This is also mediated by up-regulation of leukocyte adhesion molecules, including L-selectin, integrins, and platelet–endothelial-cell adhesion molecule 1. This also includes the up-regulation of endothelial adhesion molecules, which include E-selectin, P-selectin, intercellular adhesion molecule 1, and vascular-cell adhesion molecule1. The migration of leukocytes into the artery wall is mediated by oxidized low-density lipoprotein, monocyte chemotactic protein 1, interleukin-8, platelet-derived growth factor, macrophage colony-stimulating factor, and osteopontin.

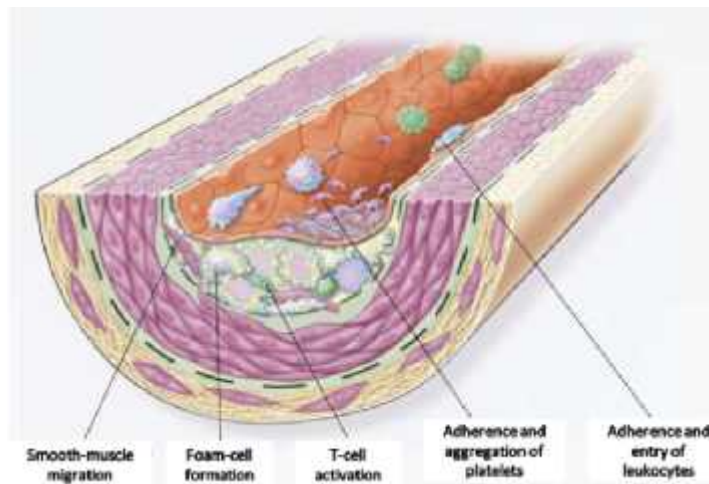


Figure 2.4 Fatty-Streak Formation in Atherosclerosis [18].

Fatty streak is formed in the artery that is the cause of further promotion of atherosclerosis, which is shown in Fig. 2.4. Fatty streaks initially consist of lipid-laden monocytes and macrophages (foam cells) together with T lymphocytes. Later they are joined by various numbers of smooth-muscle cells. The steps involved in this process include smooth-muscle migration, which is stimulated by platelet-derived growth factor, fibroblast growth factor 2, and transforming growth factor β . T-cell activation is mediated by tumor necrosis factor α , interleukin-2, and granulocyte-macrophage colony-stimulating factor. The foam cell formation is mediated by oxidized low-density lipoprotein, macrophage colony-stimulating factor, tumor necrosis factor α , and interleukin-1. The platelet adherence and aggregation are stimulated by integrins, P-selectin, fibrin, thromboxane A_2 , tissue factor, and the factors described in Fig. 2.3 as responsible for the adherence and migration of leukocytes.

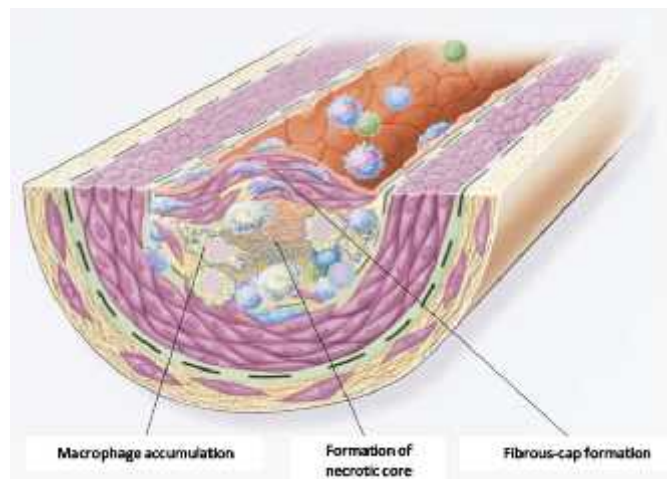


Figure 2.5 Formation of an Advanced Complicated Lesion of Atherosclerosis [18].

As fatty streaks progress to intermediate and advanced lesions, they tend to form a fibrous cap that walls off the lesion from the lumen. This formation of fibrous cap is shown in Fig. 2.5. This represents a type of healing or fibrous response to the injury. The fibrous cap covers a mixture of leukocytes, lipid, and debris, which may form a necrotic core. These lesions expand at their shoulders by means of continued leukocyte adhesion and entry caused by the same factors as those listed in Fig. 2.3 and Fig. 2.4. The principal factors associated with macrophage accumulation include macrophage colony-stimulating factor, monocyte-chemotactic protein 1, and oxidized low-density lipoprotein. The necrotic core represents the results of apoptosis and necrosis, increased proteolytic activity, and lipid accumulation. The fibrous cap is forming as a result of increased activity of platelet-derived growth factor, transforming growth factor β , interleukin-1, tumor necrosis factor α , and osteopontin and of decreased connective-tissue degradation.

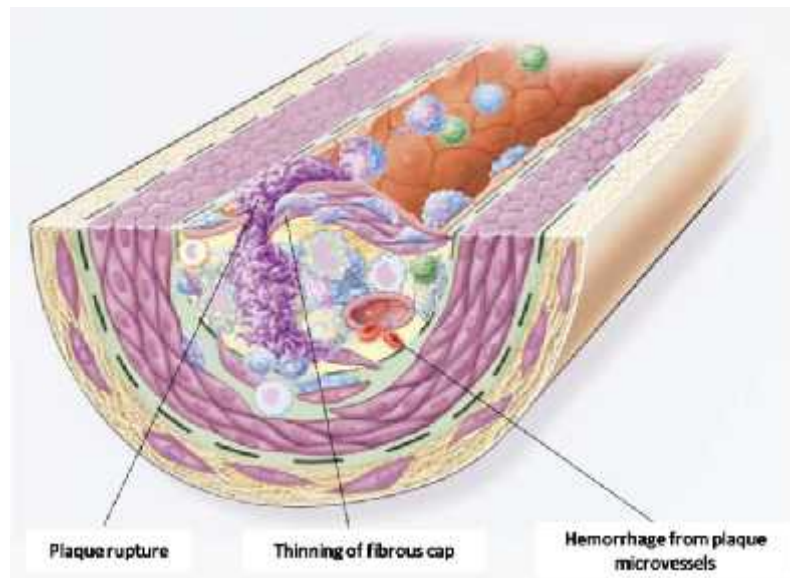


Figure 2.6 Unstable Fibrous Plaques in Atherosclerosis [18].

Rupture of the fibrous cap or ulceration of the fibrous plaque can rapidly lead to thrombosis and usually occurs at sites of thinning of the fibrous cap that covers the advanced lesion which shown in Fig. 2.6. Thinning of the fibrous cap is apparently due to the continuing influx and activation of macrophages, which release metalloproteinases and other proteolytic enzymes at these sites. These enzymes cause degradation of the matrix, which can lead to hemorrhage from the vasa vasorum or from the lumen of the artery and can result in thrombus formation and occlusion of the artery.

Artery diameter reduction due to progression of atherosclerosis is shown in Table 2.1 [37]. The comparison of Intima Media Thickness (IMT) between healthy patients and atherosclerotic patients is shown in Table 2.2 [37]. Different stenosis level is defined in Table 2.3 [37]. The blood velocity variations due to different stenosis level are shown in Table 2.4 [37].

Table 2.1 Progression of atherosclerosis

Degree of Atherosclerosis (%)	Artery Diameter Reduction (%)
Normal	None
<50	<50
50-59	50
70 but less than near occlusion	50
Near occlusion	Visible
Total occlusion	Visible, no detectable lumen

Table 2.2 Comparison of IMT between healthy patients and atherosclerotic patients

Intima Media Thickness (IMT) - mm (mean)	Females		Males	
	CCA	ICA	CCA	ICA
Healthy Patients	0.96	1.35	1.04	1.57
Patients with Atherosclerosis Disease	1.00	1.56	1.10	1.87

Table 2.3 Definition of stenosis level

Stenosis Level	Percentage of Atherosclerotic Stenosis (%)
Mild	< 50
Moderate	50-69
Severe	70-95
Critical	95-99
Obstruction	100

Table 2.4 Variation of blood velocity due to different stenosis

Degree of Stenosis	ICA mean velocity (cm/sec)	ICA/CCA velocity ratio
Normal	< 125	< 2.0
Moderate	125-230	2.0-4.0
Severe	> 230	> 4.0
Critical	High, Low or Undetectable	Variable
Obstruction	Undetectable	Not applicable
Internal Carotid Artery- ICA; Common Carotid Artery- CCA		

2.5 Relationship between Viscosity and Carotid Atherosclerosis

Blood viscosity is a measure of the thickness of blood. The thinner the blood, the less it resists flow, moving smoothly throughout the body. Increased blood viscosity is the only biological parameter that has been linked with all of the other major cardiovascular risk factors, including high blood pressure, elevated LDL cholesterol, low HDL, type-II diabetes, metabolic syndrome, obesity, smoking, age, and male gender. Whole blood is a non-Newtonian fluid, which means that its viscosity depends on shear rate. At low shear, blood cells aggregate, which induces a sharp increase in viscosity, whereas at higher shear blood cells disaggregate, deform and align in the direction of flow [38].

Atherosclerosis is now considered a chronic inflammatory disease [39], [40] and the determination of 'acute-phase' proteins has improved short- and long-term cardiovascular risk assessment in individuals with known coronary disease [41] and in apparently healthy populations [42]. A common characteristic of most 'acute-phase' proteins is that they increase red blood cell (RBC) aggregation [43] and hence RBC aggregation has been used for many years as a marker of systemic inflammation [44], [45]. Because increased RBC aggregation raises whole blood viscosity, particularly at low shear rate, whole blood viscosity is generally found to be increased in patients with atherosclerosis [46]. Levels of whole blood and plasma

viscosity predict future cardiovascular events, both short [47] and long term, [48] confirming the linkage between viscosity and the level of 'acute-phase' proteins. Blood viscosity itself has been proposed to play a pathophysiological role in atherogenesis [49]-[51].

At the sites of severe atherosclerotic obstructions or at vasospastic locations, when change of vessel diameter is limited, blood viscosity contributes to stenotic resistance thereby jeopardising tissue perfusion. However, blood viscosity plays its most important role in the microcirculation where it contributes significantly to peripheral resistance and may cause sludging in the post capillary venules. Apart from the direct hemodynamic significance, an increase in blood viscosity is also associated with increased thrombotic risk, as has been demonstrated in atrial fibrillation. Furthermore, as increased red blood cell aggregation is a reflection of inflammation, hyperviscosity has been shown to be a marker of inflammatory activity. That means hyperviscosity is the root cause of the pre-inflammatory injury that triggers endothelial dysfunction and sets in motion a cascade of events that result in the hardening and thickening of arterial walls. So, the blood viscosity is proportionally related to the carotid atherosclerosis.

2.6 Summary

This chapter has presented knowledge about human circulatory system and an overview of carotid atherosclerosis and the biological phenomena behind the cause and promotion of atherosclerosis. We have also known about the relationship between blood viscosity and carotid atherosclerosis and its growth.

CHAPTER III

Basics of Hemodynamics

Chapter Outlines

- ❖ Introduction
- ❖ Definition of Hemodynamics
- ❖ Types of Blood Flow
- ❖ Blood Flow Physics
- ❖ Computational Fluid Dynamics (CFD)
- ❖ Finite Element Method
- ❖ Summary

CHAPTER III

Basics of Hemodynamics

3.1 Introduction

Hemodynamics is the analysis of blood flow and the factors which can influence it. In clinical settings, hemodynamics is a very important part of patient assessment, because a healthy flow of blood throughout the body is critical to a patient's well being. A significant majority of all cardiovascular diseases and disorders like stroke and heart attack is related to systemic hemodynamic dysfunction. A number of factors can play a role in how well the blood travels the body, and one of the goals of clinical treatment is to make a patient hemodynamically stable, or to keep a patient hemodynamically stable if his or her blood flow has not been compromised. This chapter will discuss the concept of hemodynamics, physics of blood flow and blood pressure. This chapter will explain different types of blood flow also. Here we will know about the concept of computational fluid dynamics (CFD) and finite element method (FEM).

3.2 Definition of Hemodynamics

Blood is a suspension of cells in fluid called plasma. Blood cells occupy around 50% in volume of whole blood while plasma consists of water (92% by volume), proteins, glucose, mineral ions, hormones, carbon dioxide. Blood cells are composed of erythrocytes (RBCs), leukocytes (also called white blood cells or WBCs) and thrombocytes (PLTs). RBCs are the most abundant cells in blood and contain the hemoglobin protein which binds to oxygen and allows for its transport throughout the body. Plasma behaves as a Newtonian fluid but whole blood shows a remarkable non-Newtonian behavior consisting of shear-thinning, thixotropy and viscoelasticity [52], [53]. RBC-RBC interactions and RBC-protein interactions are the primary cause of the non-Newtonian behavior: the aggregation and disaggregation of RBCs and their deformation dictate the value of viscosity [54], [55]. A fluid is Newtonian only if the tensors that describe the viscous stress and the strain rate are related by a constant viscosity tensor that does not depend on the stress state and velocity of the flow. In a Newtonian fluid, the relation between the shear stress and the shear rate is linear, passing through the origin, the

constant of proportionality being the coefficient of viscosity. Fluids which do not obey the Newton's law of viscosity are called as non-Newtonian fluids. In reality most fluids are non-Newtonian, which means that their viscosity is dependent on shear rate or the deformation history. In contrast to Newtonian fluids, non-Newtonian fluids display either a non-linear relation between shear stress and shear rate, have a yield stress, or viscosity that is dependent on time or deformation history (or a combination of all the above). In a non-Newtonian fluid, the relation between the shear stress and the shear rate is different and can even be time-dependent. Therefore, a constant coefficient of viscosity cannot be defined.

Hemodynamics (hemo + dynamics) is the fluid dynamics of blood flow. It is an important part of cardiovascular physiology dealing with the forces the pump (the heart) has to develop to circulate blood through the cardiovascular system. Adequate blood circulation (blood flow) is necessary for adequate supply of oxygen to all tissues, which, in return, is synonymous with cardiovascular health, survival of surgical patients, longevity and quality of life. To an outside observer these hemodynamic forces demonstrate themselves as blood pressure and blood flow paired values at different nodes of the cardiovascular system. We will concentrate on systemic hemodynamics - the blood pressure and blood flow at the output of the left heart. A significant majority of all cardiovascular diseases and disorders like stroke and heart attack is related to systemic hemodynamic dysfunction. Hemodynamic response continuously monitors and adjusts to conditions in the body and its environment. Thus hemodynamics explains the physical laws that govern the flow of blood in the blood vessels. The relationships can be challenging because blood vessels are complex, with many ways for blood to enter and exit under changing conditions.

3.3 Types of Blood Flow

This section will give a brief overview of several important flow patterns.

In fluid mechanics, incompressible flow refers to a flow in which the material density is constant within a fluid parcel, an infinitesimal volume that moves with the flow velocity. An equivalent statement that implies incompressibility is that the divergence of the flow velocity is zero. Compressible flow (gas dynamics) is the branch of fluid mechanics that deals with flows having significant changes in fluid density. Gases, but not liquids, display such

behavior. That means the density is a non-constant function of the pressure, the temperature, phase, composition, etc. Therefore, blood is considered as incompressible fluid.

Laminar flow is the normal condition for blood flow throughout most of the circulatory system. It is characterized by concentric layers of blood moving in parallel down the length of a blood vessel. The highest velocity (V_{\max}) is found in the center of the vessel. The lowest velocity ($V=0$) is found along the vessel wall. The flow profile is parabolic once laminar flow is fully developed. This occurs in long, straight blood vessels, under steady flow conditions. One practical implication of parabolic, laminar flow is that when flow velocity is measured using a Doppler flowmeter, the velocity value represents the average velocity of a cross-section of the vessel, not the maximal velocity found in the center of the flow stream. The orderly movement of adjacent layers of blood flow through a vessel helps to reduce energy losses in the flowing blood by minimizing viscous interactions between the adjacent layers of blood and the wall of the blood vessel. Disruption of laminar flow leads to turbulence and increased energy losses. Laminar and Turbulent flows can be characterized and quantified using Reynolds Number (R_e). The equation for Reynolds number is:

$$R_e = \frac{\rho \cdot v \cdot D}{\mu} \quad (3.1)$$

Where v = mean velocity, D = vessel diameter, ρ = blood density, and μ = blood viscosity

Reynolds Number is directly proportional to velocity and inversely proportional to viscosity.

The Reynolds Number for laminar flow is $R_e < 2000$.

Though, generally blood flow is laminar in the body, under conditions of high flow, particularly in the ascending aorta, laminar flow can be disrupted and become turbulent. When this occurs, blood does not flow linearly and smoothly in adjacent layers, but instead the flow can be described as being chaotic. Turbulent flow also occurs in large arteries at branch points, in diseased and narrowed (stenotic) arteries and across stenotic heart valves. Turbulence increases the energy required to drive blood flow because turbulence increases the loss of energy in the form of friction, which generates heat. Turbulence does not begin to occur until the velocity of flow becomes high enough that the flow lamina breaks apart. Therefore, as blood flow velocity increases in a blood vessel or across a heart valve, there is not a gradual

increase in turbulence. Instead, turbulence occurs when a critical Reynolds number (Re) is exceeded. Reynolds number is a way to predict under ideal conditions when turbulence will occur. The Reynolds Number for turbulent flow is $Re > 4000$.

The cardiovascular system of chordate animals is a very good example where pulsatile flow is found. In fluid dynamics, a flow with periodic variations is known as pulsatile flow. The flow in the human body is generated by the pulsatile action of the heart, and a pulsatile rather than steady flow is encountered throughout the circulatory system. The velocity at a point in a vessel is, therefore, dependent on time and experiences acceleration and deceleration. This affects the velocity profile, which cannot be considered parabolic, even when a steady state of pulsation is reached. Poiseuille's law can be reformulated for pulsatile flow by assuming linearity, i.e., that the flow pattern can be decomposed into sinusoidal components and then added to obtain the velocity variation in time and space.

3.4 Blood Flow Physics

Blood flow, which is the quantity of blood that passes a given point in the circulation in a given period of time through a blood vessel has complex flow pattern. It is determined by two factors:

1. Pressure difference between two ends of the vessel, which is the force that pushes the blood through the vessel
2. Vascular resistance.

The flow through the vessel can be calculated by Ohm's law:

$$F = \frac{\zeta P}{R} \quad (3.2)$$

in which F is blood flow, ζP is the pressure difference ($P_1 - P_2$) between the two ends of the vessel, and R is the resistance.

Pressure has a great effect on blood flow, because an increase in arterial pressure, not only increases the force that pushes blood through the vessels but also swells the vessels at the same time, which decreases vascular resistance. Thus, greater pressure increases the flow in both of these ways [56].

Navier-Stokes equations describe the mechanics of fluid flow. They state the dynamical balance between the internal forces due to pressure and viscosity of the fluid and the externally applied forces. Considering isothermal conditions the time dependent incompressible blood flow is governed by the momentum and mass conservation equations, the Navier-Stokes equations given as:

$$\rho \frac{du}{dt} + \nabla \cdot \sigma = \rho f \quad (3.3)$$

where u and σ are the velocity and the stress fields, ρ the blood density and f the volume force per unit mass of fluid.

This equation system can be solved for the velocity and the pressure given appropriate boundary and initial conditions. These equations along with the conservation of energy equation form a set of coupled, nonlinear partial differential equations. It is not possible to solve these equations analytically for most engineering problems. However, it is possible to obtain approximate computer-based solutions to the governing equations for a variety of engineering problems. This is the subject matter of finite element method (FEM) and computational fluid dynamics (CFD).

3.5 Computational Fluid Dynamics (CFD)

Computational fluid dynamics, usually abbreviated as CFD, is a branch of fluid mechanics that uses numerical analysis and algorithms to solve and analyze the problems that involve fluid flows. Computational fluid dynamics (CFD) is concerned with the efficient numerical solution of the partial differential equations that describe fluid dynamics. CFD techniques are commonly used in the many areas of engineering where fluid behavior is an important factor. CFD is commonly used in applied mathematics with powerful computer to model fluid flow situations for the prediction of heat, mass and momentum transfer and optimal design in industrial processes [57]. In design and development, CFD programs are now considered to be standard numerical tools which predict not only fluid flow behavior, but also the transfer of heat, mass (such as in perspiration or dissolution), phase change (such as in freezing, melting or boiling), chemical reaction (such as combustion or rusting), mechanical movement (such as an impeller turning, pistons, fans or rudders) and stress or deformation of related solid

structures (such as a mast bending in the wind). Furthermore, CFD has been applied to deal with problems in environment and architecture. CFD has grown from a mathematical curiosity to become an essential tool in almost every branch of fluid dynamics. In biomedical applications CFD is now a day's used to model the flow of blood in the heart and vessels. The use of CFD reduces the need for tests on human being and animals until the last stage of the processing.

CFD techniques have emerged with the advent of digital computers. Since then, a large number of numerical methods have been developed to solve flow problems using this method. The purpose of a flow simulation is to find out how the flow behaves in a given system for a given set of inlet-outlet conditions. These conditions are generally termed as boundary conditions.

To solve fluid dynamics problem, we should know the physical properties of fluid. Then we can use mathematical equations to describe these physical properties. This is Navier-Stokes equation and it is the governing equation of CFD. Analytical solution of Navier-Stokes is really difficult to solve in paper. But if we want to solve this equation by computer, we have to translate it to the discretized form. The translators are numerical discretization methods, such as Finite Difference, Finite Element, Finite Volume methods. Consequently, we also need to divide our whole problem domain into many small parts because our discretization is based on them. These points are usually connected together in what is called numerical grid or mesh. The system of differential equations representing the system is converted, using some procedures, to a system of algebraic equations representing the interdependency of the flow at those points and their neighboring points. The resulting system of algebraic equations, which can be linear or non linear is usually large and requires a digital computer to solve. In essence, we end up with the unknowns being the flow quantities at the grid points. Solution of the systems results in the knowledge of these quantities at the grid points. With the development of fast validated numerical approaches, and the continuous increase in computer speed and availabilities in cheap memory, larger and larger problems are being solved using CFD methods at cheaper costs and quick turnaround times. Figure 3.1 shows the process of CFD.

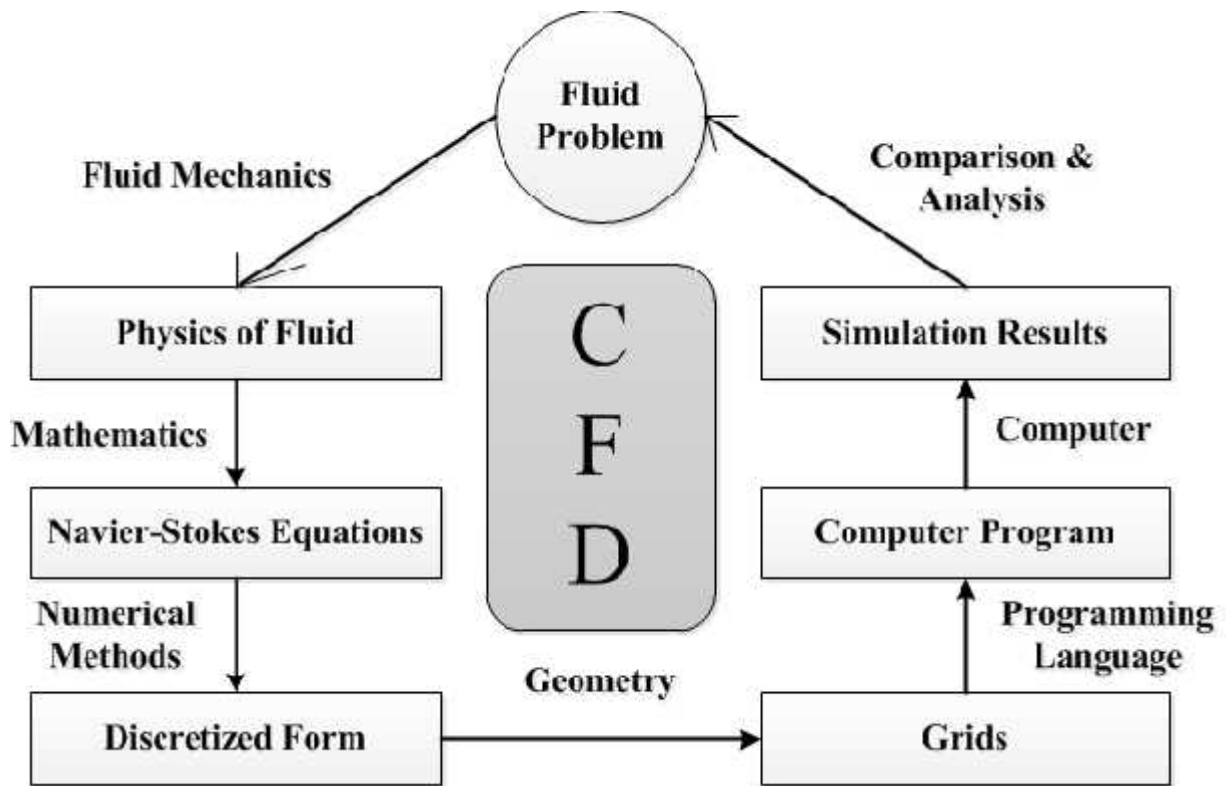


Figure 3.1 Process of Computational Fluid Dynamics

3.6 Finite Element Method

Today the finite element method (FEM) is considered as one of the well established and convenient technique for the computer solution of complex problems in different fields of engineering: civil engineering, mechanical engineering, nuclear engineering, biomedical engineering, hydrodynamics, heat conduction, geo-mechanics, etc. From other side, FEM can be examined as a powerful tool for the approximate solution of differential equations describing different physical processes.

The success of FEM is based largely on the basic finite element procedures used: the formulation of the problem in variational form, the finite element discretization of this formulation and the effective solution of the resulting finite element equations. These basic steps are the same whichever problem is considered and together with the use of the digital computer present a quite natural approach to engineering analysis.

In mathematics, the finite element method (FEM) is a numerical technique for finding approximate solutions to boundary value problems for partial differential equations. It uses

subdivision of a whole problem domain into simpler parts, called finite elements, and variational methods from the calculus of variations to solve the problem by minimizing an associated error function. Analogous to the idea that connecting many tiny straight lines can approximate a larger circle, FEM encompasses methods for connecting many simple element equations over many small subdomains, named finite elements, to approximate a more complex equation over a larger domain. FEM is best understood from its practical application, known as finite element analysis (FEA). FEA as applied in engineering is a computational tool for performing engineering analysis. It includes the use of mesh generation techniques for dividing a complex problem into small elements, as well as the use of software program coded with FEM algorithm. In applying FEA, the complex problem is usually a physical system with the underlying physics such as the Euler-Bernoulli beam equation, the heat equation, or the Navier-Stokes equations expressed in either PDE or integral equations, while the divided small elements of the complex problem represent different areas in the physical system [58].

The finite element method (FEM) is the dominant discretization technique in structural mechanics. The basic concept in the physical interpretation of the FEM is the subdivision of the mathematical model into disjoint (non-overlapping) components of simple geometry called finite elements or elements for short. The response of each element is expressed in terms of a finite number of degrees of freedom characterized as the value of an unknown function, or functions, at a set of nodal points. The response of the mathematical model is then considered to be approximated by that of the discrete model obtained by connecting or assembling the collection of all elements. Because FEM is a discretization method, the number of degrees of freedom of a FEM model is necessarily finite. They are collected in a column vector called u . This vector is generally called the DOF vector or state vector. The term nodal displacement vector for u is reserved to mechanical applications. FEM solution process is like as:

1. Divide structure into pieces (elements with nodes) (discretization/meshing).
2. Connect (assemble) the elements at the nodes to form an approximate system of equations for the whole structure (forming element matrices).
3. Solve the system of equations involving unknown quantities at the nodes (e.g., displacements).
4. Calculate desired quantities (e.g., strains and stresses) at selected elements.

3.7 Summary

This chapter has introduced us to knowledge about the hemodynamics, the fluid dynamics of blood flow. We have known about the blood flow physics and blood pressure. We have acquired knowledge about the Newtonian and Non-Newtonian fluid and also compressible and incompressible flow along with other flow types. We have also known about the computational fluid dynamics techniques (CFD) and finite element method (FEM) through which we can simulate blood flow dynamics in carotid artery.

CHAPTER IV

Basics of Ultrasound Flow Imaging

Chapter Outlines

- ❖ Introduction
- ❖ Evolution of Ultrasound Imaging
- ❖ Generation of Ultrasound Pulses
- ❖ Ultrasound Wavelength and Frequency
- ❖ Measurement of Flow Signals
- ❖ Simulation of Flow Imaging System
- ❖ Velocity Estimation Using Doppler Method
- ❖ Velocity Estimation Using Autocorrelation Algorithm
- ❖ Color Flow Mapping Using Cross Correlation
- ❖ Summary

CHAPTER IV

Basics of Ultrasound Flow Imaging

4.1 Introduction

Ultrasound flow imaging is one where ultrasound signal is used for visualizing the moving particle in human body. This chapter introduces the concept of ultrasound flow imaging. The clinical world has greatly benefited from these safe, fast and interactive systems for studying the human circulation. The development of these scanners continues and new methods for vector velocity imaging are on the verge of being introduced. They will add new information to the field allowing the detailed study of complex flow. This chapter gives an explanation on the interaction between the ultrasound and the moving blood. The calculation of the velocity distribution is then explained along with the different physical effects influencing the estimation. The simulation of these flow systems using spatial impulse responses is described. Finally the estimation of mean velocities for color flow mapping is also described.

4.2 Evolution of Ultrasound Imaging

Ultrasound has been used to image the human body for over half a century. Dr. Karl Theo Dussik, an Austrian neurologist was the first to apply ultrasound as a medical diagnostic tool to image the brain [59]. Today ultrasound (US) is one of the most widely used imaging technologies in medicine. It is portable, free of radiation risk, non-invasive, painless and relatively inexpensive when compared with other imaging modalities, such as magnetic resonance and computed tomography. It has real time scanning capability comparing with other imaging modalities. Velocity estimation in medical ultrasound has had a long history since the early work of Satomura [60] on continuous wave Doppler to color flow mapping introduced by Namekawa *et al.* [61] and Kasai *et al.* [62]. In mid 1950s, where an experiments performed by Satomura, in Japan demonstrated that continuous wave (CW) ultrasound was capable of detecting motion. CW ultrasound cannot locate the depth of the motion and several pulsed wave solutions were therefore made by Baker, Peronneau and Leger, and Wells around 1970. From these early experimental systems the scanners have now evolved into systems for

routine use in nearly all hospitals, and ultrasound is one of the most common means of diagnosing hemodynamic problems today.

4.3 Generation of Ultrasound Pulses

Ultrasound transducers (or probes) contain multiple piezoelectric crystals which are interconnected electronically and vibrate in response to an applied electric current. This phenomenon called the piezoelectric effect was originally described by the Curie brothers in 1880 when they subjected a cut piece of quartz to mechanical stress generating an electric charge on the surface [63]. Later, they also demonstrated the reverse piezoelectric effect, i.e., electricity application to the quartz resulting in quartz vibration [64]. These vibrating mechanical sound waves create alternating areas of compression and rarefaction when propagating through body tissues. Sound waves can be described in terms of their frequency (measured in cycles per second or hertz), wavelength (measured in millimeter), and amplitude (measured in decibel).

4.4 Ultrasound Wavelength and Frequency

The wavelength and frequency of US are inversely related, i.e., ultrasound of high frequency has a short wavelength and vice versa. US waves have frequencies that exceed the upper limit for audible human hearing, i.e., greater than 20 kHz [60]. Medical ultrasound devices use sound waves in the range of 1–20 MHz. Proper selection of transducer frequency is an important concept for providing optimal image resolution in diagnostic and procedural US. High-frequency ultrasound waves (short wavelength) generate images of high axial resolution. Increasing the number of waves of compression and rarefaction for a given distance can more accurately discriminate between two separate structures along the axial plane of wave propagation. However, high-frequency waves are more attenuated than lower frequency waves for a given distance; thus, they are suitable for imaging mainly superficial structures [65].

Conversely, low-frequency waves (long wavelength) offer images of lower resolution but can penetrate to deeper structures due to a lower degree of attenuation (Fig. 4.1). For this reason, it is best to use high frequency transducers (up to 10–15 MHz range) to image superficial structures (such as for satellite ganglion blocks) and low-frequency transducers (typically 2–5 MHz) for imaging the lumbar neuraxial structures that are deep in most adults (Fig. 4.2).

Ultrasound waves are generated in pulses (intermittent trains of pressure) that commonly consist of two or three sound cycles of the same frequency (Fig. 4.3).

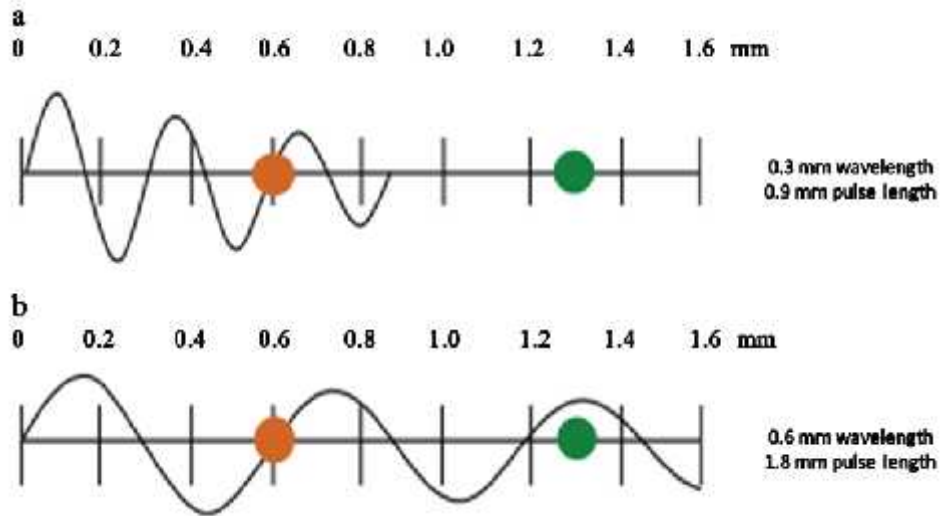


Figure 4.1 Attenuation of ultrasound waves and its relationship to wave frequency.

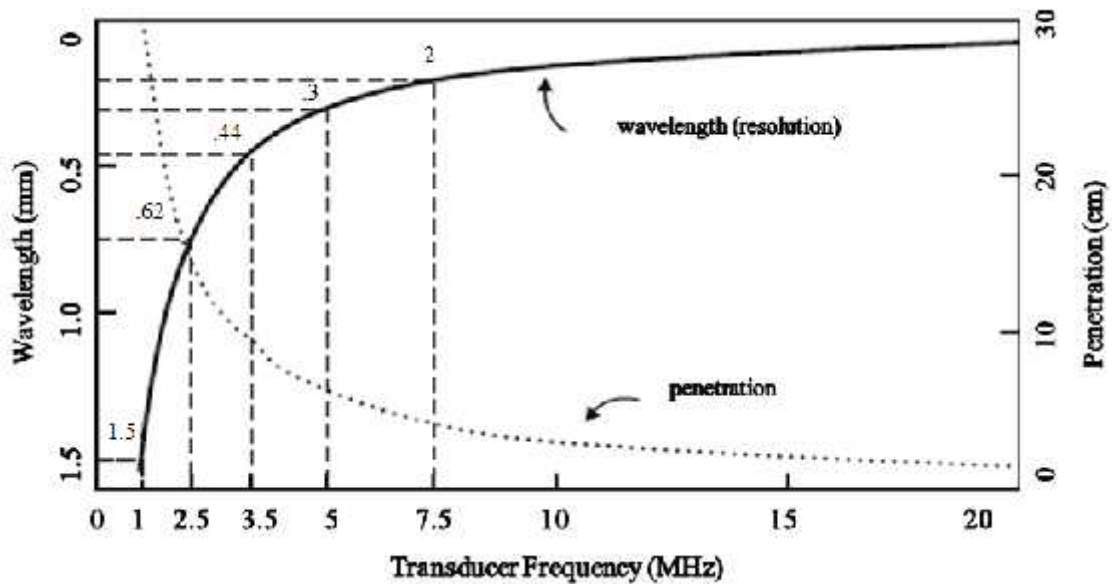


Figure 4.2 A comparison of the resolution and penetration of different ultrasound transducer frequencies [60].

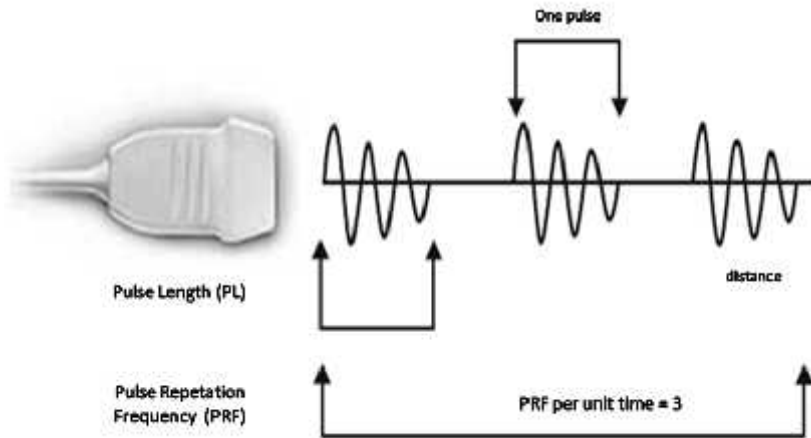


Figure 4.3 Schematic representation of ultrasound pulse generation [66].

Note that higher frequency waves are more highly attenuated than lower frequency waves for a given distance. Reproduced from ref. [67] pulse repetition frequency (PRF) is the number of pulses emitted by the transducer per unit of time. Ultrasound waves must be emitted in pulses with sufficient time in between to allow the signal to reach the target of interest and be reflected back to the transducer as echo before the next pulse is generated. The PRF for medical imaging devices ranges from 1 to 10 kHz.

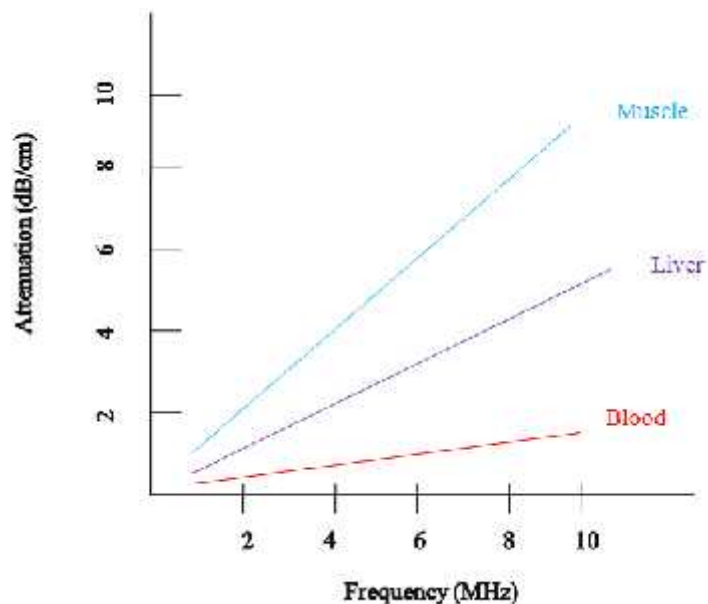


Figure 4.4 Degrees of attenuation of ultrasound beams as a function of the wave frequency in different body tissues [67].

All ultrasound equipment intrinsically compensates for an expected average degree of attenuation by automatically increasing the gain (overall brightness or intensity of signals) in deeper areas of the screen. Fluid-containing structures attenuate sound much less than solid structures so that the strength of the sound pulse is greater after passing through fluid than through an equivalent amount of solid tissue.

4.5 Measurement of Flow Signals

The data for the velocity measurement is obtained by emitting a short ultrasound pulse with 4 to 8 cycles at a frequency of 2 to 10 MHz. The ultrasound is then scattered in all directions by the blood particles and part of the scattered signal is received by the transducer and converted to a voltage signal. The blood velocity is found through the repeated measurement at a particular location. The blood particles will then pass through the measurement gate and give rise to a signal with a frequency proportional to velocity. A coordinate system for the measurement is shown in Fig. 4.5. The vector \vec{r}_1 indicates the position for one scatterer, when the first ultrasound pulse interacts with the scatterer. The vector \vec{r}_2 indicates the position for interaction with the next ultrasound pulse emitted T_{prf} seconds later. The movement of the scatterer in the z-direction away from the transducer in the time interval between the two pulses is

$$D_z = \frac{2 \cos \theta}{c} \frac{d}{dt} \left(\frac{2 \cos \theta}{c} \right) \vec{V} \cdot \vec{T}_{prf} \quad (4.1)$$

where θ is the angle between the ultrasound beam and the particle's velocity vector \vec{V} .

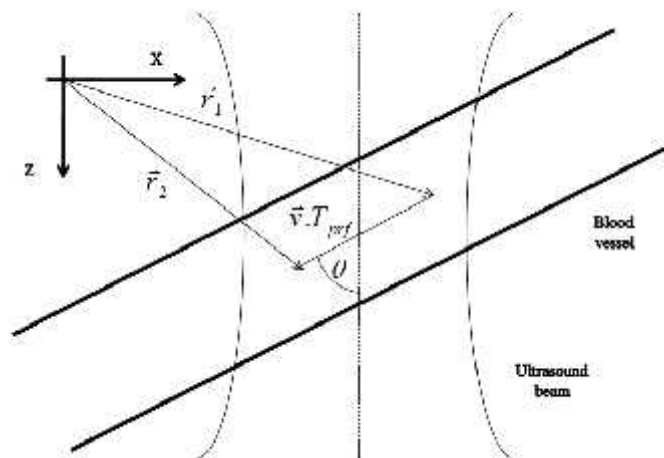


Figure 4.5 Coordinate system for finding the movement of blood particles.

The traveled distance gives rise to a delay in the second signal compared to the first. Denoting the first received signal as $r_1(t)$ and the second as $r_2(t)$ gives,

$$r_1(t) \approx r_2(t - \Delta t) \quad (4.2)$$

$$\Delta t = \frac{2D_z}{c} - \frac{2|\vec{V}| \cos \theta}{c} T_{prf} = \frac{2V_z}{c} T_{prf}; \quad (4.3)$$

where c is the speed of sound. Emitting a sinusoidal pulse $p(t)$ with a frequency of f_0 gives a received signal of

$$p(t) \approx g(t) \sin(2\pi f_0 t) \text{ for } 0 < t < M/f_0; \quad (4.4)$$

$$r_1(t) \approx p(t - t_0) \quad (4.5)$$

$$t_0 = \frac{2d}{c}; \quad (4.6)$$

where d is the depth of interrogation, and $g(t)$ is the envelope of the pulse.

Repeating the measurement a number of times gives a received, sampled signal for a fixed depth of

$$r_i(t_x) \approx p(t_x - t_0 - \Delta t_s) \approx g(t_x - t_0 - \Delta t_s) \sin(2\pi f_0 (t_x - t_0 - \Delta t_s)) \quad (4.7)$$

Here, t is time relative to the pulse emission. Taking the measurement at the same time t_x relative to the pulse emission corresponding to a fixed depth in tissue gives

$$r_i(t_x) \approx g(t_x - t_0 - \Delta t_s) \sin(2\pi f_0 (t_x - t_0 - \Delta t_s)) \quad (4.8)$$

$$\tau_x = \frac{2d}{c} \quad (4.9)$$

Assuming the measurement is taken at times when the envelope $g(t)$ of the pulse is constant. Such a measurement will yield one sample for each pulse-echo RF line, and thus samples the slow movement of the blood scatterers past the measurement position or range gate as shown in Fig. 4.6. The sampled signal $r(i)$ can be written as:

$$r(i) \approx \sin(2\pi f_0 \frac{2V_z}{c} i T_{prf} - \Gamma \tau_x) \quad (4.10)$$

Showing that the frequency of this signal is:

$$f_p \times \frac{2V_z}{c} f_0 \quad (4.11)$$

which is proportional to the projected velocity of the blood in the direction of the ultrasound beam.

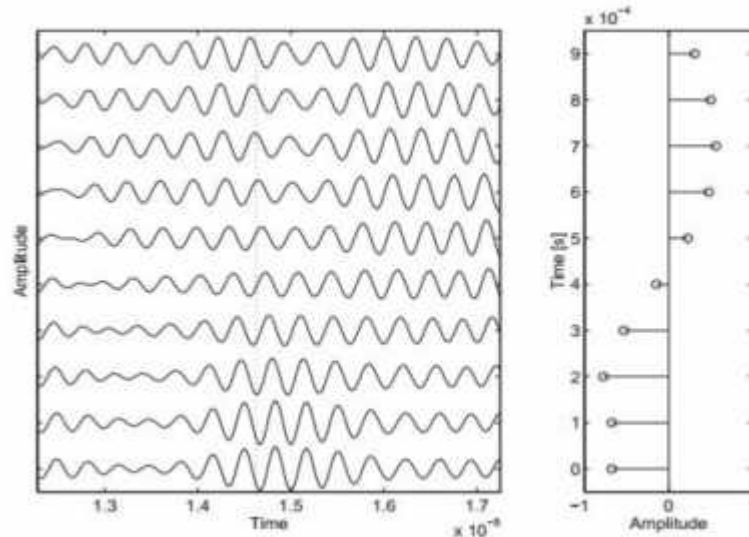


Figure 4.6 RF sampling of simulated signal from blood vessel. (The left graph shows the different received RF lines, and the right graph is the sampled signal.)

The velocity can be both towards and away from the transducer, and this should also be included in the estimation of velocity. The sign can be found by using a pulse with a one-sided spectrum corresponding to a complex signal with a Hilbert transform relation between the imaginary and real part of the signal. The one sided spectrum is then scaled by $2V_z/c$ and has a unique peak in the spectrum from which the velocity can be found. The complex signal can be made by Hilbert transforming the received signal and using this for the imaginary part of the signal. A Hilbert transform is difficult to make with analog electronics and two other implementations are shown in Fig. 4.7. The top graph makes the demodulation by a complex multiplication with $\exp(j2f_0t)$ and then low pass filtration for removing the peak in the spectrum at $2f_0$. Matching the bandwidth of the low-pass filters to the bandwidth of the pulse also gives an improvement in signal-to-noise ratio. The second solution obtains the signal by quadrature sampling with a quarter wave delay between the two channels. Both

implementations give complex signals that can readily be used in the estimators for determining the velocity with a correct sign [68].

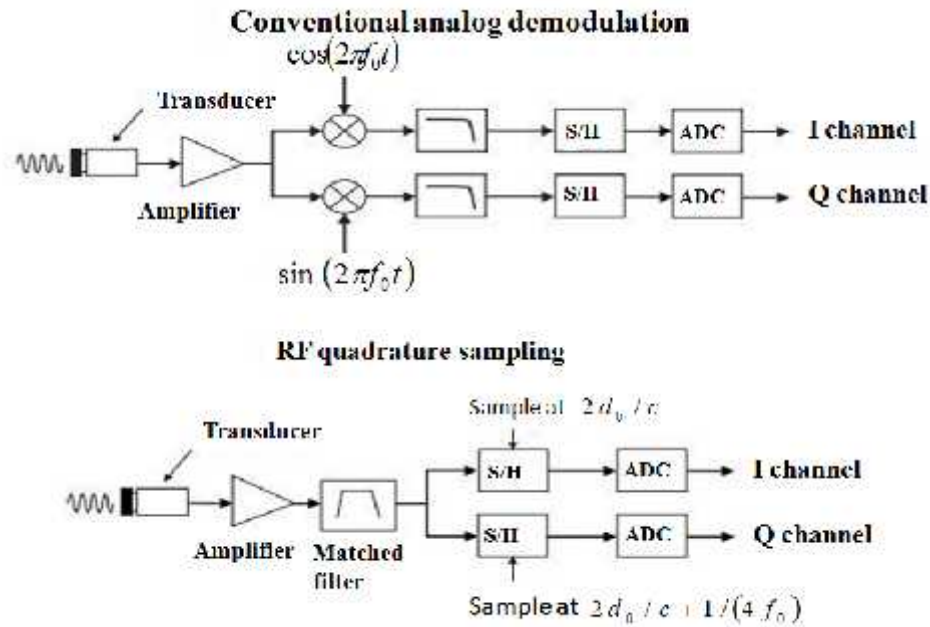


Figure 4.7 Demodulation schemes for obtaining a complex signal for determining the sign of the velocity.

4.6 Simulation of Flow Imaging System

The derivation given in this section generally assumes that the single scatterer stays within a region of uniform insonation. Both continuous and pulsed fields vary with position and this needs to be taken into account using the Tupholme–Stepanishen field model.

$$\text{The received voltage trace, } p_r \bar{r}_1, \bar{r}_2, t \text{ A X } V_{pe} \bar{f}_t \text{ A}^* \bar{f}_m \bar{r}_1 \text{ A}^* h_{pe} \bar{r}_1, \bar{r}_2, t \text{ A} \quad (4.12)$$

where f_m accounts for the scattering by the medium, h_{pe} describes the spatial distribution of the ultrasound field, and V_{pe} is the one-dimensional pulse emanating from the pulse excitation and conversion from voltage to pressure and back again. The scatterer will move during the interaction with the ultrasound giving rise to a Doppler shift. The most important feature is, however, the inter pulse movement, because this is used by the pulsed scanners for detecting velocity. The approximation is then to include the small Doppler shift into the one-dimensional pulse V_{pe} , shifting its frequency content to $f \hat{=} (1 + 2V_z/c)f$, and assuming that the field interacting with the scatterer stays constant. Usually the pulse duration is a few

microseconds, so that the scatterers only move a fraction of a millimeter, even for high blood velocities, during the interaction, and the field can safely be assumed to be constant over this distance. The received voltage trace is then found directly from above equation with \vec{r}_2 indicating the position of the scatterers. Note that a spatial convolution takes place and that the received response is a summation of contributions from numerous scatterers. The scatterers move to the position:

$$\vec{r}_2 + \vec{f}_i \Gamma \Delta X - \vec{r}_2 + \vec{f}_i \Gamma \Delta T_{prf} + V \vec{f}_2 \vec{f}_i \Delta t \quad (4.13)$$

when the next field from the subsequent pulse emission impinges on the scatterers. Here ‘ i ’ denotes the pulse or line number and $V \vec{f}_2 \vec{f}_i \Delta t$ is the velocity of the scatterer at the position indicated by $\vec{r}_2 + \vec{f}_i \Gamma \Delta t$ at time ‘ t ’. This assumes that the scatterers do not accelerate during the interaction. The movement between pulses is $T_{prf} V \vec{f}_2 \vec{f}_i \Delta t$, and the new position of the scatterers, $\vec{r}_2 + \vec{f}_i \Gamma \Delta t$, can then be inserted and used for calculating the next voltage trace. The received signals for multiple pulse emissions can, thus, be found by these two equations. The actual calculation is rather complicated in three dimensions, but is easy to handle by a computer. The different velocities for the scatterers necessitate that separate Doppler shifts are included in V_{pe} for each scatterer. This can be done in a computer simulation of each scatterer before the contributions for all scatterers are summed, or a mean Doppler shift can be used. The effect of this Doppler shift is minor in pulsed systems and can, at least to a first approximation, be neglected. A fairly realistic simulation should, thus, be possible with this approach.

4.7 Velocity Estimation Using Doppler Method

Doppler ultrasound is an important noninvasive technique for measuring blood velocity in order to diagnose cardiovascular diseases. The pulsed Doppler technique is widely used at the present time because it also offers range resolution. With this method, sequential short ultrasound pulses are transmitted into the vessel or heart at the pulse repetition frequency (PRF). Returned signals are received sequentially at a certain delay after the pulse transmission. The blood velocity within selected ranges can be estimated from the received signal. Sweeping the beam across the vessel gives a complete measurement of a 2-D flow profile in the vessel which includes velocity and its variance. A color flow image is obtained

by coding the velocities. The velocity variance also has been used to modulate the color in some display modes.

Most widely used velocity estimation methods are the autocorrelation technique (AM). The AM technique was first developed for weather radar applications and applied to ultrasound blood velocity measurement later [69]. It is based on the phase estimation for successive pulses from the complex demodulated signal.

The correlation function plays an important role in the estimation of blood velocity parameters. Most velocity estimators are based on the correlation function. This is because the received blood signal is a Gaussian random signal [70] which is completely characterized by its correlation function [71]. Therefore, the blood velocity parameters are included in the correlation function. Here, a 2D correlation function model based on [72] is introduced.

The received 2D RF signal is denoted as $p(t,k)$ where t is the elapsed time after pulse transmission which corresponds to a certain depth from the transducer and k is the pulse number. Its correlation function is defined by the statistical ensemble average of the signal product:

$$R_{p(t,k)p^*(t,k)} = \langle p(t,k)p^*(t,k) \rangle \quad (4.14)$$

Assuming that $f(t) \cos(\tilde{S}_0 t)$ is the transmitted pulse, where $r(t)$ is the envelope of the transmitted signal, \tilde{S}_0 is transmitted center frequency, and assuming that $s(t) \cos(\tilde{S}_c t)$ is the received signal from a single scatterer, where $e(t)$ is the envelope of the received pulse and \tilde{S}_c is the mean frequency of the received pulse. The function $e(t)$ is determined by the convolution of the envelope of the transmitted pulse, the impulse response of transmission and reception transducer. The mean frequency of the received pulse may be different from the center frequency of transmitted pulse. This is because, when there is the effect of the frequency dependent attenuation and frequency random fluctuation, the envelope and the center frequency of the received pulse are altered [73]. The major effect is a shift in the spectral mean. Thus, the effect to the envelope will be neglected. The mean frequency is shifted from \tilde{S}_0 to \tilde{S}_c .

When the effect of the beam profile is taken into account and $b(d)$ is the transverse beam sensitivity function, where d is the distance from the ultrasonic beam center axis, the received pulse is: $s(t)b(d)$. This is based on the assumption of separability of the radial and transverse

impulse response [72]. With the stationary and uniform velocity field assumption, the RF correlation function is given by:

$$R_e(\tau) = \int_{-\infty}^{\infty} \int_{-\infty}^{\infty} R_e(t) R_e(t + \tau) \cos\left(\frac{2\pi v \cos \theta \tau}{c}\right) R_B(d) \sin \theta \, dt \, dd \quad (4.15)$$

$R_e(\tau)$ is the correlation function of $e(t)$ and $R_B(d) \sin \theta$ is the correlation function of lateral sensitivity function $B(d)$.

$$\tau = \frac{2v \cos \theta \tau}{c} \quad (4.16)$$

τ is the delay between echoes from two subsequent pulses caused by the scatterer movement, $v \cos \theta$ and $v \sin \theta$ are the velocity components in the radial (along the ultrasonic beam) and the lateral (transversal to the ultrasonic beam) direction. T is the pulse repetition period. The radial velocity toward the transducer is defined as positive velocity. Note that the autocorrelation model in equation (4.15) includes decorrelation caused by lateral velocity components. Decorrelation caused by velocity gradients may be included by integrating equation (4.15) over the corresponding velocity distribution.

In the conventional autocorrelation method (AM), the complex correlation function with lag one in the temporal direction is used to calculate the normalized mean frequency [74]. Using the notation for the 2-D correlation function, the normalized mean frequency in the temporal direction is estimated as [75]:

$$\% \text{X phase } f_{R_x} = f_0 \quad (4.17)$$

From the Doppler equation, the velocity estimate is calculated, assuming that the center frequency of the received signal is constant and equal to the transmitted frequency f_0

$$v = \frac{c \% \text{PRF}}{4 f f_0 \cos \theta} \quad (4.18)$$

Frequency dependent attenuation and frequency random fluctuation effects cause variations in the received signal center frequency. This results in velocity bias and estimation variance. The effect of the frequency-dependent attenuation becomes significant especially in the wideband signals. This effect can be reduced by estimating the center frequency of the received signal f_c and using it for the estimation,

$$v = \frac{c \% \text{PRF}}{4 f f_c \cos \theta} \quad (4.19)$$

The deviation of the received signal center frequency $\zeta f_c - f_0$ is estimated from the autocorrelation function with lag in the depth range direction:

$$\zeta f_c - f_0 = \frac{\text{phase} \{ R_x(f, 0) \}}{2f_0} \quad (4.20)$$

This method is referred to as ‘‘AM with frequency compensation’’ and also is described in [75] and [76].

4.8 Velocity Estimation Using Autocorrelation Algorithm

The most common method to detect the velocity is to measure the change in phase $\frac{d\omega}{dt}$ by acquiring multiple vectors (i.e. V_e, V_{e+1} and V_{e+2} in Fig. 4.8) along a single scan line with the transducer stationary, and then calculate the average change in phase at each range bin along the scan line [74]. This method is called autocorrelation method.

To illustrate the basics of the autocorrelation method, an enveloped monochromatic, continuous time signal is assumed. The Hilbert transform is employed to create a complex signal.

$$r_{rec}(t) = x(t) + jy\hat{x}(t) \quad (4.21)$$

The complex signal can be written as

$$r_{rec}(t) = g(t) \exp \left[j \left(2\pi f_0 t + \frac{2v_z}{c} Z \right) \right] \quad (4.22)$$

$$x(t) = g(t) \exp \left[j \omega t \right]$$

Here $g(t)$ is the envelope function and the phase ωt is related to the axial velocity and the velocity is proportional to the phase derivative given by

$$\frac{d\omega}{dt} = 4\pi f_0 \frac{v_z}{c} \quad (4.23)$$

and the velocity is

$$v_z = \frac{c}{4f_0} \frac{d\omega}{dt} \quad (4.24)$$

Thus, the velocity v_z is estimated through an estimate of phase derivative of the received signal.

The phase of the complex signal is

$$\omega t A \arctan \frac{y f t A}{x f t A} \quad (4.25)$$

Barber et.al. [77] showed that computing the first lag of autocorrelation is sufficient to correctly estimate the change in phase $\frac{d\omega f t A}{dt}$ for each range bin t :

$$\frac{d\omega f t A}{dt} \arctan \frac{\frac{E Z Z}{e X 0} \bullet y_e f t A_{e \Gamma} f t A Z x_e f t A_{e \Gamma} f t A}{\frac{E Z Z}{e X 0} \bullet x_e f t A_{e \Gamma} f t A \Gamma y_e f t A_{e \Gamma} f t A} \quad (4.26)$$

where the denominator and numerator are respectively the real and imaginary part of the first lag of autocorrelation, and E is the ensemble size, varying from 4 to 16.

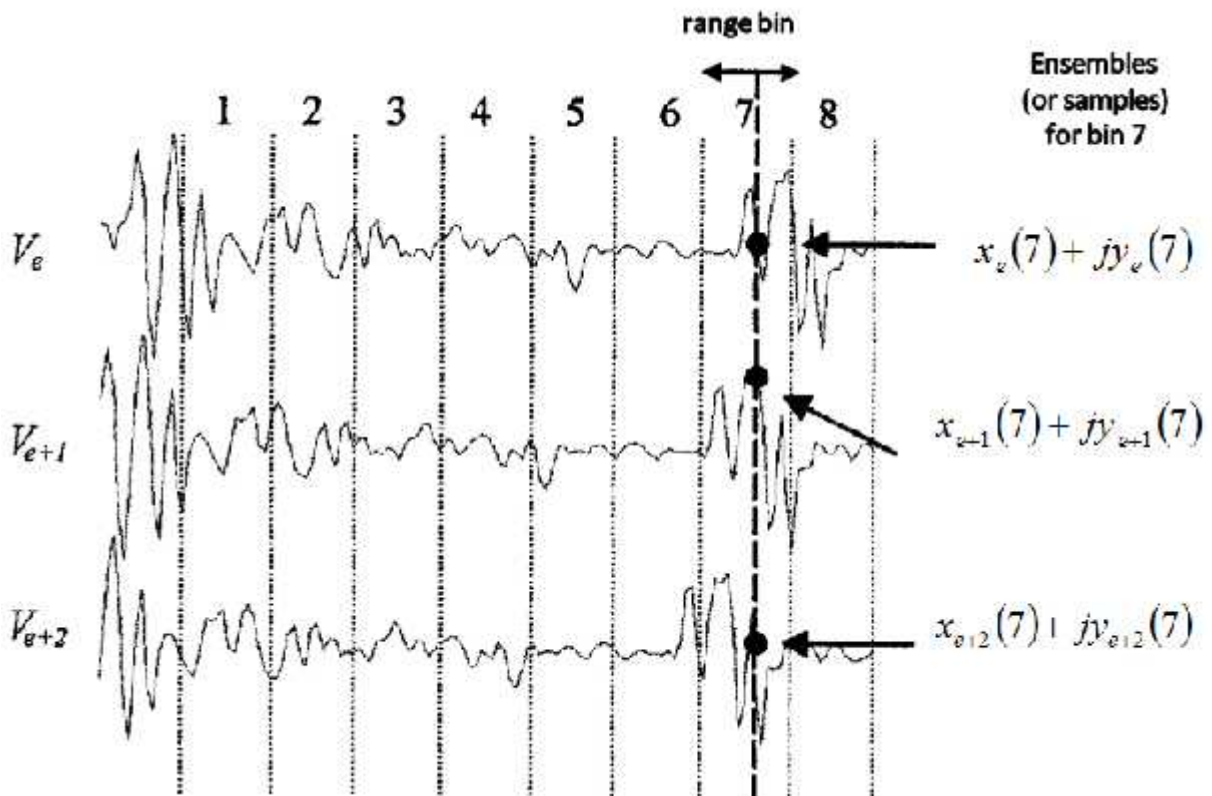


Figure 4.8 Example of autocorrelation velocity estimate [74].

In Figure 4.8, the waveforms of the three vectors appear to be moving to the left (toward the transducer) over time. Three ensemble samples after demodulation, i.e. $x_e f t A_e \Gamma y_e f t A_e$, for the 7th range bin are used to illustrate the data needed to estimate $\frac{dW_e f t A_e}{dt}$ for this range bin.

If the time between the recorded line is T_{prf} . The velocity is expressed as

$$v_z = \frac{c}{4f f_0 T_{prf}} \arctan \frac{\frac{E_{z0}^{Z2}}{e_{x0}} \bullet y_e f t A_e \Gamma z_e f t A_e \Gamma x_e f t A_e \Gamma y_e f t A_e}{\frac{E_{z0}^{Z2}}{e_{x0}} \bullet x_e f t A_e \Gamma z_e f t A_e \Gamma y_e f t A_e \Gamma x_e f t A_e} \quad (4.27)$$

Thus the phase contributions from several lines are averaged.

4.9 Color Flow Mapping Using Cross Correlation

The estimation of velocity can also be done by finding the time-shift between two consecutive RF signals directly [78]-[80]. The principle of cross-correlation based velocity estimation can be understood from the Fig. 4.9.

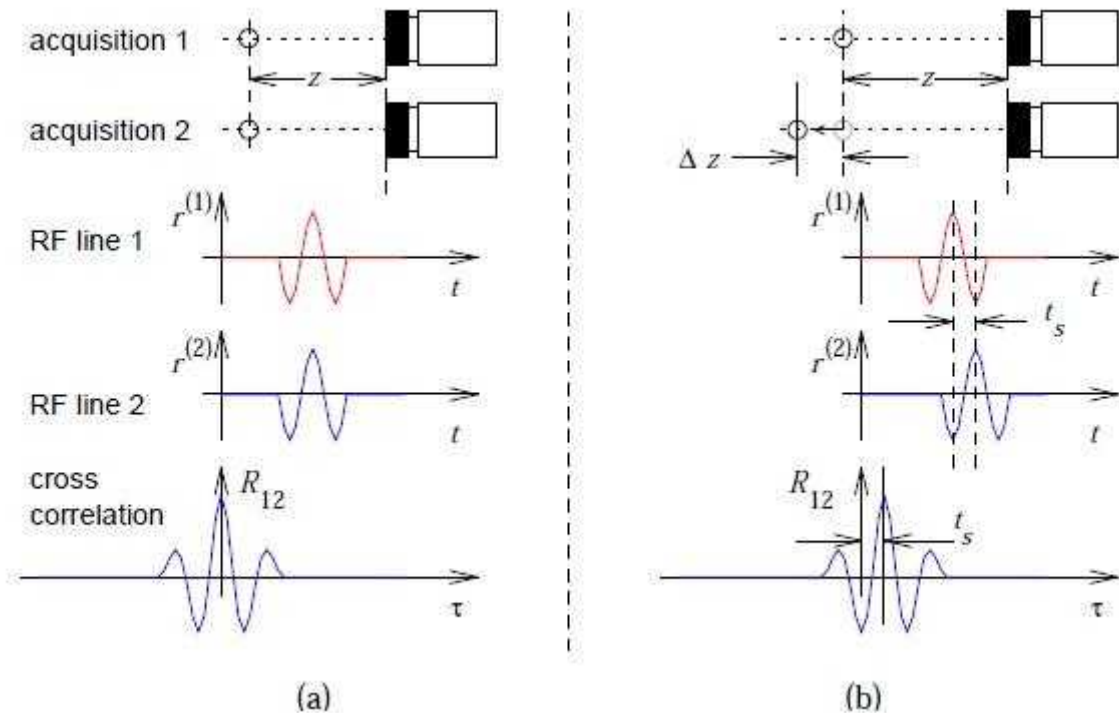


Figure 4.9 Principle of velocity estimation using cross-correlation

The received RF signal is amplified and filtered with a matched filter to remove noise. An RF sampling at 20 to 30 MHz for a 5 MHz transducer is then performed and the removal of

stationary signals is done by subtracting two consecutive RF lines. Velocity is estimated by a one-dimensional correlation between the RF echo vectors (i.e. V_e , V_{e+1} and V_{e+2} in Fig. 4.10) collected from consecutively transmitted ultrasonic pulses along the same beam line. The vectors are divided into several range bins as shown in Fig. 4.10. The cross-correlation is calculated first:

$$R_{\tau, i} = \frac{1}{N} \sum_{n=0}^{N-1} V_{e, i}^* V_{e+1, i+n} \quad (4.28)$$

where τ is the number of lags, i denotes the bin number, and N is the number of samples in a bin.

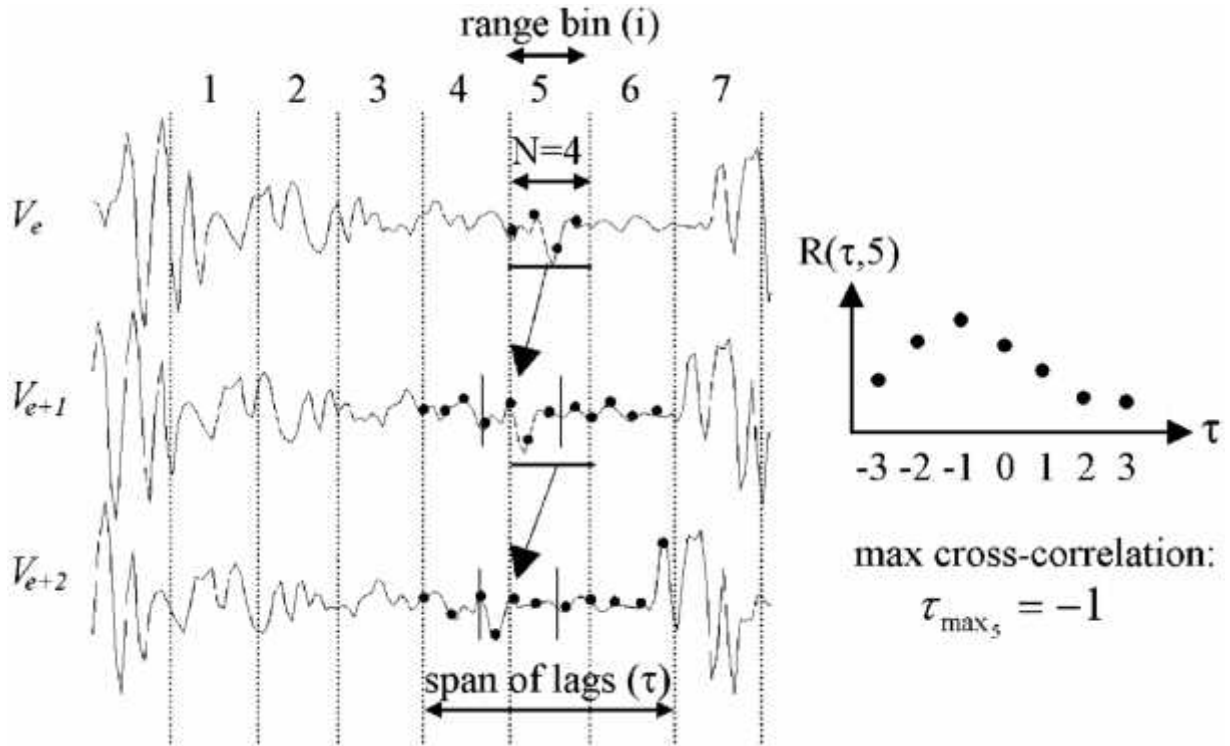


Figure 4.10 Example of cross-correlation velocity estimate [74].

The velocity at the corresponding bin is

$$v = \frac{c}{2} \frac{\tau_{\max, i}}{f_s} \cdot PRF \quad (4.29)$$

where $\tau_{\max, i}$ is the lag at which the maximum correlation occurred for the i th range bin and f_s is the RF sampling frequency, which is fourfold or more the center frequency of the transducer for proper sampling [68].

The cross-correlation approach is optimized by sending out a narrow pulse, which also makes it easier to obtain a higher resolution in the color flow mapping images. The price is, however, that the peak intensities must be limited due to the safety limits imposed on the scanners. Therefore cross-correlation scanners can send out less energy and are often less sensitive than the scanners using the autocorrelation approach.

Another disadvantage of the cross-correlation approach is the large amount of calculations that must be performed per second. For a real time system it can approach one billion calculations per second making it necessary to use only the sign of the signals in the calculation of the cross-correlation [81].

4.10 Summary

This chapter has introduced us to know about the basics of ultrasound flow imaging systems. From this section, we have known about the ultrasound signal frequency and wavelength and attenuation of ultrasound signals by different body tissues. We have known about the concept of interaction between ultrasound beam and blood particle. We have also gathered knowledge about auto and cross-correlation algorithm for blood velocity measurement and finally for color flow velocity image.

CHAPTER V

Simulation Methodology

Chapter Outlines

- ❖ Introduction
- ❖ Simulation Strategy
- ❖ Simulation of Blood Flow Using CFD
- ❖ Ultrasound Signal Simulation for Flow Imaging
- ❖ Summary

CHAPTER V

Simulation Methodology

5.1 Introduction

Atherosclerosis in carotid artery can be studied using computational fluid dynamics concept. Investigation on the evolution of atherosclerotic diseases in the carotid artery is our major consideration. A better understanding can be achieved through computer simulation of the blood flow model of stenosis in carotid artery bifurcation. Simulation is the imitation of the operation of a real-world process or system over time. Simulating something first requires a model which represents the key characteristics or behaviors/functions of the selected physical system or process. This chapter describes the simulation of velocity images of different models for blood flow through cardiovascular vessels using realist CFD and effective ultrasound techniques. Then the ultrasound based flows images will be compared with CFD references and investigated to enhance the quality of the images.

5.2 Simulation Strategy

The simulation work in this study has two fold: one is the CFD part and another is the ultrasound based detection using CFD data. Using a combination of computational fluid dynamics and finite element analysis techniques allows one to study the physics involved with atherosclerosis. Then taking the numerically computed displacement, velocity and geometry information, and effective methods will be applied to simulate ultrasound color flow images. In this study, we apply finite element method to solve the blood flow model. We have used CFD to solve differential equations of fluid flows numerically which is an effective technique for computing blood flow data. The position of the scatterers for multiple times instant is necessary for velocity estimation. The flow estimation can be done from the shifting information of the scatterers using ultrasound RF signals. The flowchart of the simulation methodology is shown in the Fig. 5.1.

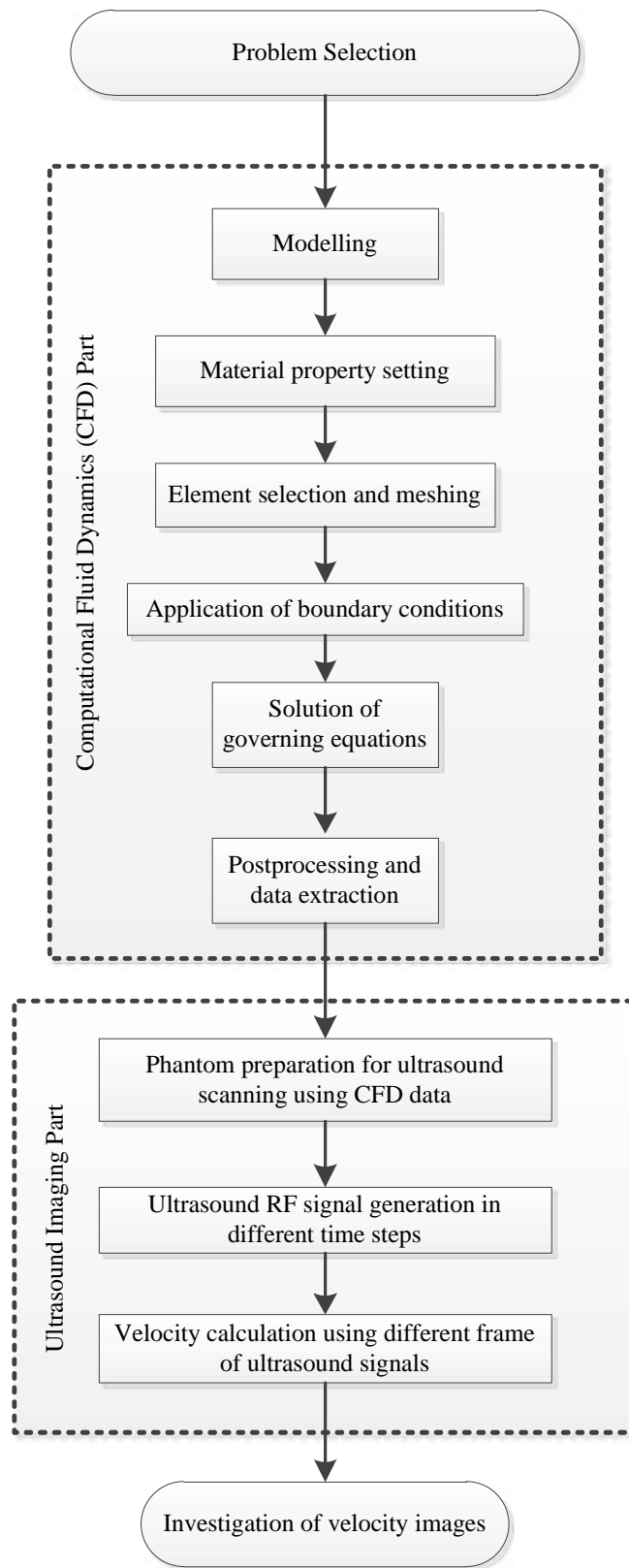


Figure 5.1 Flow chart of simulation strategy

5.3 Simulation of Blood Flow Using CFD

The blood in artery is assumed to be incompressible, laminar and non-Newtonian fluid governed by Navier-Stokes equations as explained in Chapter 3. Three models with different cases have been considered relating to normal carotid and carotid atherosclerosis cases. Carotid stenosis is caused by a buildup of plaque inside the artery wall that reduces blood flow to the brain which is called atherosclerosis. Carotid atherosclerosis is a major risk factor for brain stroke and can lead to brain damage.

A fixed density considering the realistic density of blood and variable viscosity related to carotid atherosclerosis has been chosen for the analysis. The artery wall is assumed to be rigid and a parabolic velocity profile as an inlet boundary condition. The outlet boundary is defined considering pressure as degree of freedom. All wall boundary layers were defined as no-slip walls, resulting in a zero velocity along the wall surface. In this study, the biochemical and mechanical interactions between blood and vascular tissue are neglected. In an elderly person the walls of the arteries thicken, lose their elasticity, become stiffer and the effects of wall compliance can be neglected. Then no slip at the interface with the rigid vessel wall can be assumed. At the flow entrance, Dirichlet boundary conditions are considered prescribing a parabolic distribution for the time dependent value of the velocity. The finite element solver has solved the time-dependent incompressible Navier- Stokes equations to compute the resultant velocities considering the blood properties and boundary conditions.

In this work, we use the popular finite element solver ANSYS software to solve blood flow model for getting FEM blood flow data. ANSYS software offers solutions for advanced multiphysics modeling by designing software that can import complex biological geometries, model complex physics interactions and perform automatic design exploration analysis, all within a single simulation environment. The integration of ANSYS Fluent into ANSYS provides users with superior bi-directional connections to all major CAD systems, powerful geometry modification and creation with ANSYS Design Modeler technology, and advanced meshing technologies in ANSYS Meshing. The combination of these benefits with the extensive range of physical modeling capabilities and the fast, accurate CFD results has made ANSYS very popular. The CFD solver ANSYS contain three main components to provide useful information; 1) pre-processor, 2) solver, and 3) post-processor. Pre-processing consists of inputting a fluid flow problem into a CFD program. This includes defining the geometry of

the region of interest, grid or mesh generation, selection of the physical and chemical phenomena that need to be modeled, a definition of fluid properties, and specification of appropriate boundary conditions at the inlet and outlet. Numerical solution techniques are available such as finite difference, finite element, finite volume, and spectral methods. Each has a distinct numerical technique, but the basis of the solver is to perform an approximation of unknown flow variables by means of simple functions, discretization by substitution of the approximations into the governing flow, and an algebraic solution. Visualization tools finally show the domain geometry and grid, vector plots, line and contour plots, surface plots, particle tracking as post processed results.

5.3.1 Carotid Artery Geometry Model

The carotid arteries are a paired set of arteries, one for each side of the body, that supply blood to the head and neck. The location most frequently affected by carotid atherosclerosis is the carotid bifurcation as shown in Fig. 5.2. The arterial structure consists of a common carotid artery (CCA), internal carotid artery (ICA), and external carotid artery (ECA). The CCA branches into the ICA and ECA at the carotid artery bifurcation. The ICA has a localized dilation at its carotid artery bifurcation origin. This dilation is known as the carotid sinus or bulb. The combination of bifurcation, curvature, pulsatility, and sudden change in arterial diameter causes the flow to be highly complex with recirculation regions and secondary flows. It is in areas of complex or disturbed flow that atherosclerosis is prominent in the vasculature.

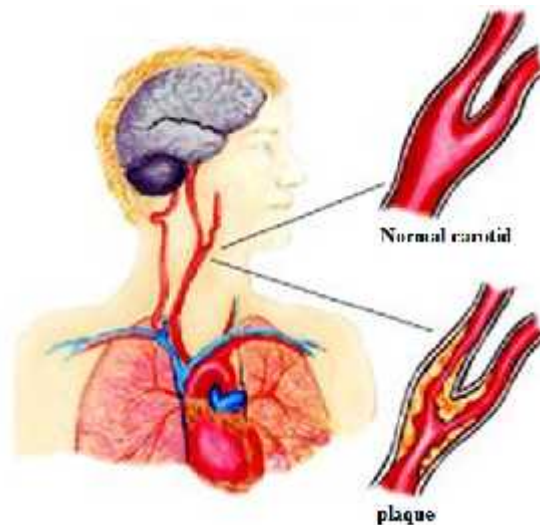


Figure 5.2 Carotid artery bifurcation [82].

Computational model carotid artery with common carotid artery (CCA), internal carotid artery (ICA) and external carotid artery (ECA) is modeled through ANSYS. Here the length of the CCA, ICA and ECA are 10 mm, 5 mm and 5 mm respectively. The diameter of the CCA, ICA and ECA are 4 mm, 3 mm and 2 mm respectively. We artificially added stenosis in the junction of internal carotid artery (ICA) and external carotid artery (ECA), which is known as carotid bifurcation region. The entry level of CCA is defined as inlet boundary and the end level of ICA and ECA are defined as outlet boundary. Fig. 5.3 shows the stenosed carotid artery bifurcation model with common carotid artery (CCA), internal carotid artery (ICA) and external carotid artery (ECA) along with their real scenarios.

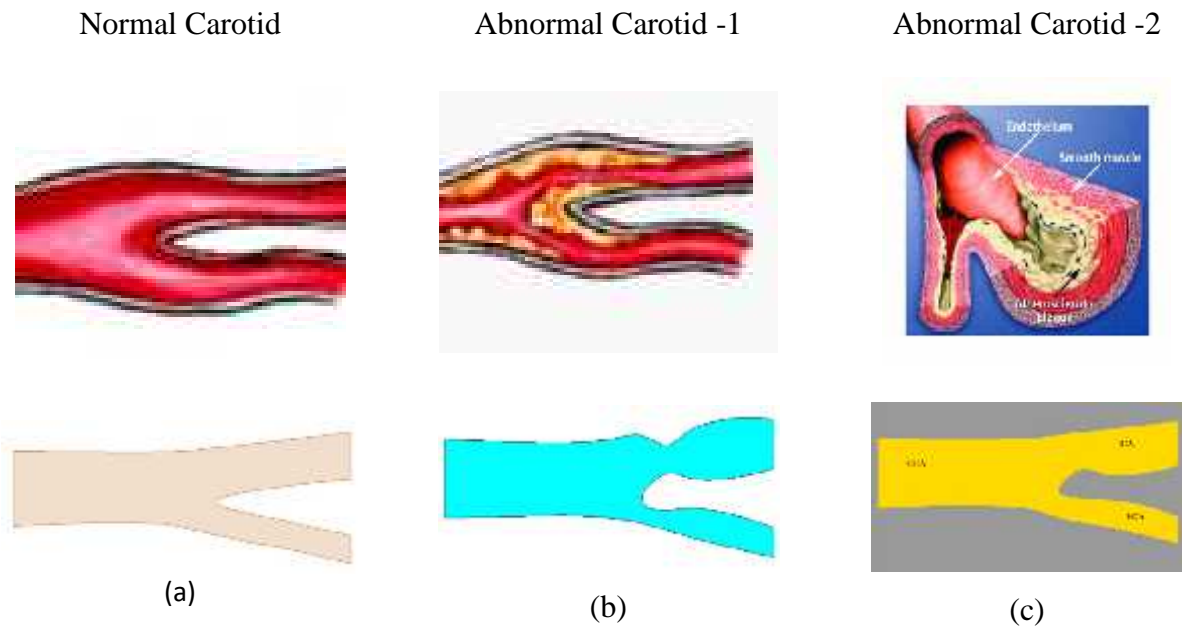


Figure 5.3 Carotid artery model for different cases

5.3.2 Material Properties for Flow Model

Blood shows marked non-Newtonian effects and proper constitutive equations able to capture these effects are required. Despite the majority of work in the biomechanical literature is still based on the Newtonian approximation, i.e. the instantaneous decrease in viscosity for increasing shear rate, has a profound influence on the flow field [83]. The non-Newtonian effects are important both at the local and the global level: size and strength of vortical structures and recirculating regions.

In this work, blood in carotid artery is assumed to be incompressible, laminar and non-Newtonian fluid. Blood flow is governed by the continuity equation (conservation of mass) for an incompressible medium and the Navier-stokes equations (conservation of momentum) which are needed to solve using CFD. A fixed density of 1060 kg/m^3 and variable viscosity of 3.5 mPa-s, 7 mPa-s and 10 mPa-s has been considered for the analysis. The incompressibility condition is employed being blood very well approximated as a perfectly incompressible material. The Reynolds numbers for three different blood viscosities with fixed blood density are shown in Table 5.1.

Table 5.1 Measurement of Reynolds numbers for three different blood viscosities

Cases	Blood viscosity (mPa-s)	Reynolds number at CCA inlet
Normal	3.5	605
Abnormal-1	3.5	605
Abnormal-2	3.5	605
	7.0	302
	10	212

5.3.3 Discretization of the Geometrical Model

Discretization process is the key part of this simulation. Discretization of the spatial volumes enclosed by the resultant surface models, forming their respective fluid domains, is carried out via commercial mesh generation software ANSYS using quadratic elements. Meshing criteria specified a maximum spacing of 0.040 mm in the well-defined laminar flow regions of the CCA inlet extension and ECA outlet extension, and a maximum spacing of 0.020 mm in the critical region encompassing the bifurcation, carotid bulb and downstream region of complex flow in the ICA branch. The resultant grid for this carotid artery geometry contained almost 17500 elements. Fig. 5.4 shows the mesh diagram of carotid artery model for normal and atherosclerosis cases.

Boundary conditions are applied to the inlet surface, the outlet surfaces and the luminal wall surface. The artery wall is assumed to be rigid and a parabolic velocity profile with a maximum velocity of 0.5 m/s is chosen as an inlet boundary condition. The outlet boundary is defined as a pressure outlet with initial pressure of 0.0 Pa. All wall boundary layers were defined as no-slip walls, resulting in a velocity of 0.0 m/s along the wall surface. The flow velocities are then computed at different central locations in the common carotid and also at internal and external carotid arteries.

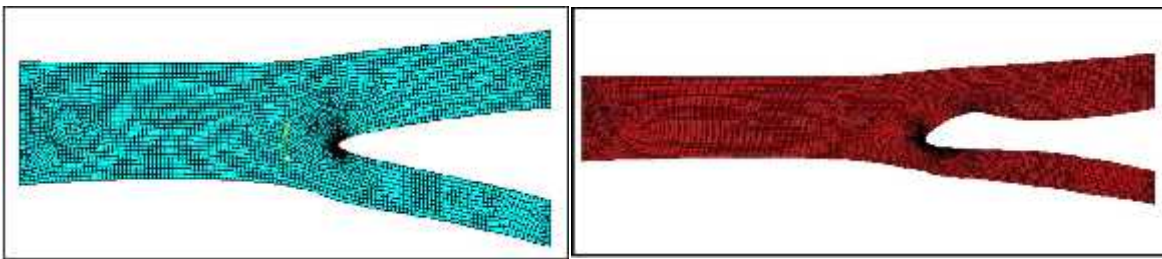


Figure 5.4 Mesh diagram of the normal and stenosed carotid artery model

5.4 Ultrasound Signal Simulation for Flow Imaging

The scattering centers (red blood cells) are taken from the FEM data to make the synthetic phantom for ultrasound imaging. The position of the scatterers for multiple times instant is necessary for velocity estimation. The flow estimation can be done from the shifting information of the scatterers using ultrasound RF signals. For ultrasound RF signals generation, we use the widely accepted ultrasound image simulation software Field II [84]-[86]. Field II allows modeling arbitrary probes and implementing realistic scanning sequences to generate RF signals for simulating ultrasound images using the model data. This version of the program runs under MATLAB and can simulate all kinds of ultrasound transducers and the associated images. The program consists of a C program and a number of Matlab m-functions that calls this program. All calculations are performed by the C program, and all data is kept by the C program. The focusing and apodization of the transducers can be controlled dynamically, and it is, thus, possible to simulate all kinds of ultrasound imaging systems.

5.4.1 The Spatial Impulse Response Concept in Field II

The Field program system uses the concept of spatial impulse responses as developed by Tupholme and Stepanishen in a series of papers [87]-[89]. The approach relies on linear systems theory to find the ultrasound field for both the pulsed and continuous wave case. This is done through the spatial impulse response. This response gives the emitted ultrasound field at a specific point in space as function of time, when the transducer is excited by a Dirac delta function. The field for any kind of excitation can then be found by just convolving the spatial impulse response with the excitation function. The impulse response will vary as a function of position relative to the transducer, hence the name spatial impulse response.

The received response from a small oscillating sphere can be found by acoustic reciprocity. The spatial impulse response equals the received response for a spherical wave emitted by a point. The total received response in pulse echo can, thus, be found by convolving the transducer excitation function with the spatial impulse response of the emitting aperture, with the spatial impulse response of the receiving aperture, and then taking into account the electromechanical transfer function of the transducer to yield the received voltage trace [84], [90].

5.4.2 Transducer

A transducer is a device that converts a signal in one form of energy to another form of energy. Energy types include (but are not limited to) electrical, mechanical, electromagnetic (including light), chemical, acoustic or thermal energy. While the term 'transducer' commonly implies the use of a sensor/detector, any device which converts energy can be considered a transducer. Ultrasound transducer (probe) produces sound waves that bounce off body tissues and make echoes. The transducer also receives the echoes and sends them to a computer that uses them to create a picture called a sonogram. Transducers (probes) come in different shapes and sizes for use in making pictures of different parts of the body. The transducer may be passed over the surface of the body or inserted into an opening such as the rectum or vagina. US transducer converts electrical energy into acoustic energy (sound) during transmission and converts acoustic energy to electrical energy during reception. Conversion is accomplished through the piezoelectric effect. 'Piezo' is Greek for 'to press' & 'elektron' is Greek for

‘amber’, refers to the property of certain crystals to emit electrical energy when pressure is applied.

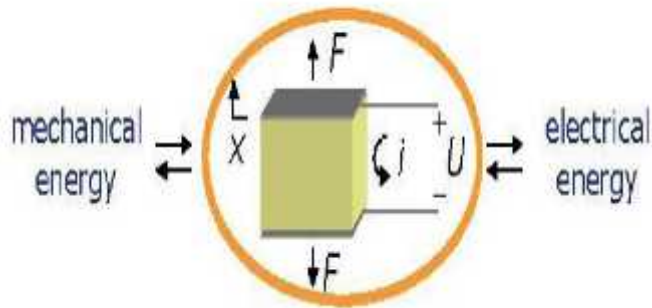


Figure 5.5 Piezoelectric & reverse piezoelectric effect [91].

In US, the crystal expands and contracts with a returning sound wave causing an electrical voltage to be emitted and returning sound wave are converted into electrical signals.

In US, voltage applied to opposite sides of the crystal cause it to expand; polarity is reversed (AC current) causing the crystal to contract. Constant change from expansion to contraction and contraction to expansion result in mechanical waves is (sound) being produced. Thus, the electrical signal is converted into a sound wave.

A number of different authors have calculated the spatial impulse response for different transducer geometries. But in general it is difficult to calculate a solution, and especially if apodization of the transducer is taken into account. Here the transducer surface does not vibrate as a piston, e.g. the edges might vibrate less than the center. The simulation program circumvents this problem by dividing the transducer surface into squares and the sum the response of these squares to yield the response. Thereby any transducer geometry and any apodization can be simulated [91]. A 16-element rectangular transducer is shown in the figure below.

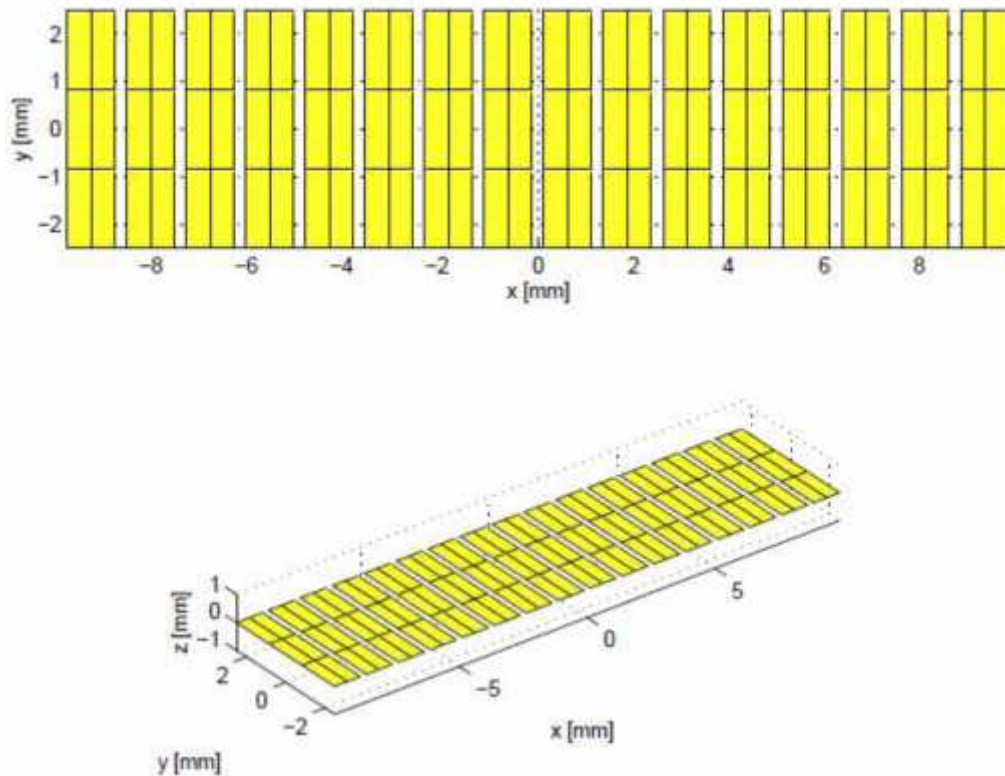


Figure 5.6 Rectangles for a 16 elements linear array transducer.

5.4.3 Sound Beam Formation

We do not want the sound beam coming from the transducer to be non-directional (diffraction) like a light bulb. Diffraction causes the sound beam to spread out as the waves move further from the transducer. We want the sound beam to be directional like a flashlight. So, the design of the transducer permits the sound beam to follow Huygens's Principle. Huygens's Principle states that "all points on a wave are considered a point source for the production of spherical secondary wavelets". These wavelets combine to produce a new wave front that determines the direction of the sound beam. The resulting effect of the destructive and constructive interference of the sound wavelets is a sound beam that is hourglass-shaped with most of the energy transmitted along the main central beam. Huygens's Principle explains why the sound beam shape does not immediately demonstrate diffraction. Sound beam produced by the transducer is hourglass-shaped. At its starting point, the sound beam is equal to transducer's diameter. As the sound travels so the width of the beam is changed. It becomes narrower until it reaches its smallest diameter; then it begins to diverge.

5.4.4 Focusing

Focusing is an important issue in ultrasound imaging. For each focal zone there is an associated focal point and the time from which this focus is used. The focusing can also be set to be dynamic, so that the focus is changed as a function of time and thereby depth. All the time values for focusing are calculated relative to a point on the aperture. Initially this is set to (0, 0, 0). This is used in linear array imaging, where the origin of the emitted and received beam is moved over the aperture. The focusing values are calculated by:

$$t_i = \frac{1}{c} \sqrt{(x_c - x_f)^2 + (y_c - y_f)^2 + (z_c - z_f)^2} - \frac{1}{c} \sqrt{(x_i - x_f)^2 + (y_i - y_f)^2 + (z_i - z_f)^2} \quad (5.1)$$

where $(x_f; y_f; z_f)$ is the position of the focal point, $(x_c; y_c; z_c)$ is the reference center point on the aperture for the focus as set by `xdc_center_focus`, $(x_i; y_i; z_i)$ is the center for the physical element number i , c is the speed of sound, and t_i is the calculated delay time. The value is then quantized, if that is set for the aperture.

The time line method is employed for the apodization, where the time decides which apodization vector is used. The vector holds one apodization value for each physical element. Frequency dependent attenuation can be included in the simulation by using the procedure `set_field`. The attenuation is included through a frequency dependent term and a frequency independent term. The frequency dependent term is linearized through a center frequency `att_f0`, so that the attenuation is zero dB at `att_f0`. Figure 5.7 illustrates the focussing concept.

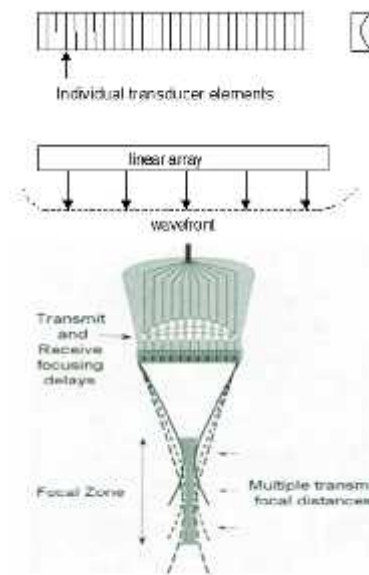


Figure 5.7 Ultrasound focusing concept [88].

There are different types of array of transducer; among them here we will discuss about three array transducers which are shown in Fig. 5.8. The linear array transducer is shown in Fig. 5.8 (a). It selects the region of investigation by firing a set of elements situated over the region. The beam is moved over the imaging region by firing sets of contiguous elements.

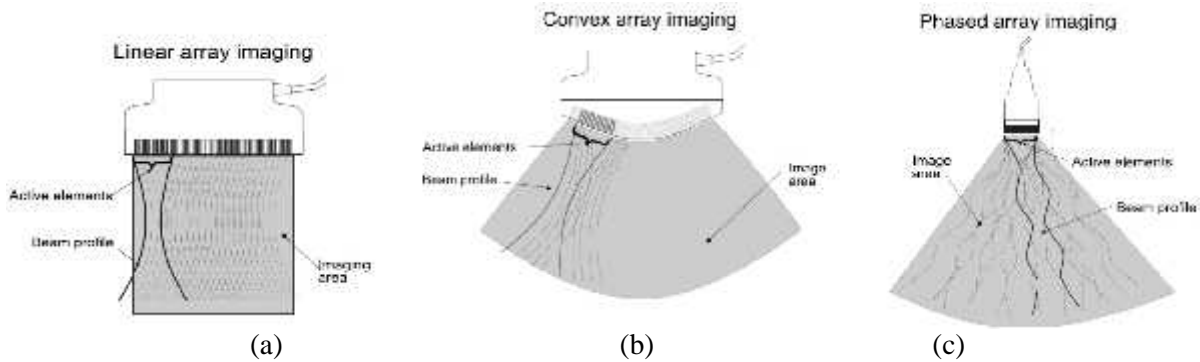


Figure 5.8 Different array of transducer (a) Linear array, (b) Convex array, and (c) Phased array.

The linear arrays acquire a rectangular image, and the arrays can be quite large to cover a sufficient region of interest (ROI). A larger area can be scanned with a smaller array, if the elements are placed on a convex surface as shown in Fig. 5.8 (b). A sector scan is then obtained. The method of focusing and beam sweeping during transmit and receive is the same as for the linear array, and a substantial number of elements (often 128 or 256) is employed.

The convex and linear arrays are often too large to image the heart when probing between the ribs. A small array size can be used and a large field of view attained by using a phased array as shown in Fig. 5.8 (c). All array elements are used here both during transmit and receive.

We have used linear array to generate the ultrasound RF signals.

5.4.5 Ultrasound Beam Simulation

We have used Field II for ultrasound beam simulation. Figure 5.9 shows the linear ultrasound transmission beam pressure at focal region with the profile at center line that has been simulated for the following settings:

Center freq. = 7.5 MHz

Speed of sound = 1540 m/s

Height of element = 5 mm

Width of element= 0.2 mm
 Dist. bet. elements = 0.02 mm
 Transmit Focus = 60 mm

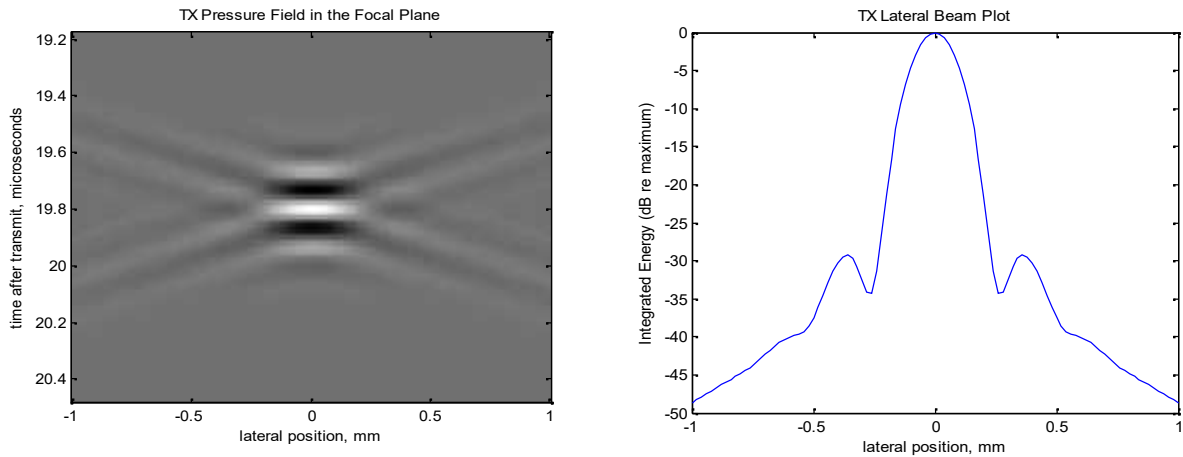


Figure 5.9 Ultrasound beam pattern crosssection.

Figure 5.10 shows the recieved response for the individual elements and the summed signal for one line. We considered 256 lines to cover the entire region of interest.

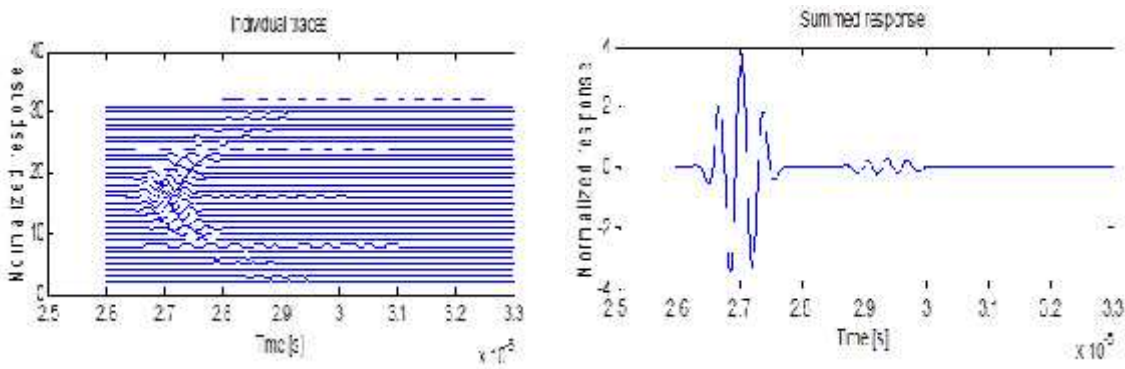


Figure 5.10 Recieved response for the individual elements and the summed signal for one line.

Figure 5.11 shows the simulated ultrasound RF signals and B-mode image for three effective points scatterers with different echogeneities.

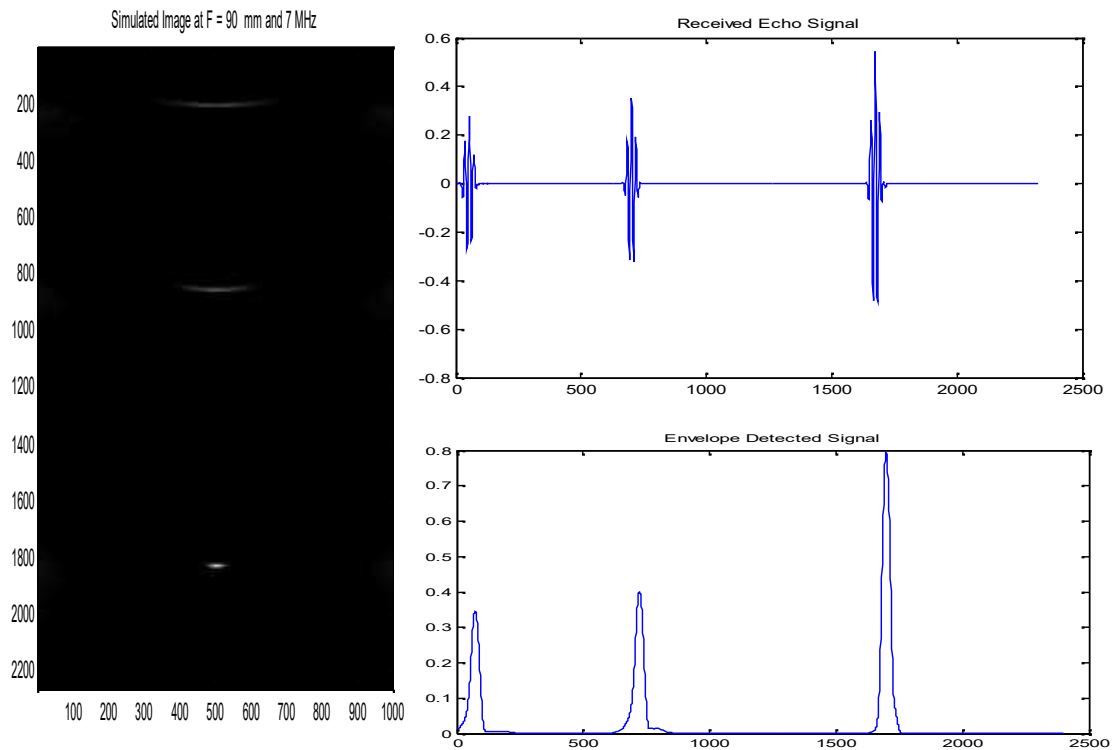


Figure 5.11 Simulated ultrasound RF signals and B-mode image for three effective points scatterers with different echogeneities.

5.4.6 Ultrasound Color Flow Image (CFI) Simulation

The color flow images reflect the projected velocity components in the direction of ultrasound beam propagation. A rate of change of phase can be interpreted as a time or frequency shift and the velocity of the target can be calculated from this information. In Field II, tissue is modeled as a collection of point scatterers. Blood can in this setting be modeled as randomly distributed point scatterers with a density that, according to the central limiting theorem, results in Gaussian-distributed RF-signal amplitudes. The total number of scatterers then needed is related to the resolution of the imaging system determined by the pulse length and the lateral and elevation beam width, which avoids the extreme computational effort needed for representing each red blood cell by separate point scatterers. Field II simulation times are mainly related to the number of point scatterers, the axial sampling frequency, and the number and shape of mathematical subelements used for modeling the transducer. The number of scatterers significantly contributing to the RF-signal is determined by the beam intensity and

can thus be reduced by including only scatterers in the vicinity of the main lobe without significantly affecting results [72]. The Nyquist criterion determines in theory the axial sampling frequency. However, a higher sampling frequency is typically necessary to represent the simulated spatial impulse responses [92].

We set a linear probe with 5MHz center frequency and 100MHz sampling rate was modeled. 256 RF lines were simulated using 128 transducer elements of which 64 active elements firing with focal length to cover the phantom. Hanning apodization is used to transmit and receive aperture. We have considered 10 time steps to generate RF signals for each frame using CFD data of 10 time steps.

Dynamic objects are achieved by moving the point scatterers during simulation. Each ultrasound beam is simulated individually, and it is therefore possible to update the position of moving scatterers between beam acquisitions using the autocorrelation based phase estimation. The envelope (Inphase and Quadrature) of the received signal has been obtained using Hilbert transform. Then the IQ signals are auto-correlated to estimate the phase shift as described below.

The Hilbert transform introduce a 90-degree phase shift to all sinusoidal components. In the discrete-time periodic-frequency domain, the transfer function of Hilbert transform is specified as follows,

$$H(j\omega) = \begin{cases} -j, & \omega > 0 \\ j, & \omega < 0 \\ 0, & \omega = 0 \end{cases} \quad (5.2)$$

The convolution kernel for $H(j\omega)$ can be calculated through inverse Fourier transform:

$$h(t) = \frac{1}{2\pi} \int_{-\infty}^{\infty} H(j\omega) e^{j\omega t} d\omega$$

$$= \frac{2}{\pi} \int_0^{\infty} \frac{\sin^2(\omega t)}{\omega} d\omega \quad (5.3)$$

Finally the velocities are computed from the phase shift information.

The velocity v_z is estimated through an estimate of phase derivative of the received signal. The phase of the complex signal is

$$w_{ft} \arctan \frac{y_{ft}}{x_{ft}} \quad (5.4)$$

As described in chapter 4, the computation of first lag of autocorrelation is sufficient to correctly estimate the change in phase $\frac{dw_{ft}}{dt}$ for each range bin t :

$$\frac{dw_{ft}}{dt} \arctan \frac{\sum_{e \in X}^{EZ} y_e \Delta_{e\Gamma} \Delta Z x_e \Delta_{e\Gamma}}{\sum_{e \in X}^{EZ} x_e \Delta_{e\Gamma} \Delta \Gamma y_e \Delta_{e\Gamma}} \quad (5.5)$$

where the denominator and numerator are respectively the real and imaginary part of the first lag of autocorrelation, and E is the ensemble size, varying from 4 to 16.

In the Figure 4.8 of previous chapter-4, the waveforms of the three vectors appear to be moving to the left (toward the transducer) over time. Three ensemble samples after demodulation, i.e. x_{ft} and y_{ft} , for the 7th range bin are used to illustrate the data needed to estimate $\frac{dw_{ft}}{dt}$ for this range bin.

If the time between the recorded line is T_{prf} . The velocity is expressed as

$$v_z = \frac{c}{4ff_0 T_{prf}} \arctan \frac{\sum_{e \in X}^{EZ} y_e \Delta_{e\Gamma} \Delta Z x_e \Delta_{e\Gamma}}{\sum_{e \in X}^{EZ} x_e \Delta_{e\Gamma} \Delta \Gamma y_e \Delta_{e\Gamma}} \quad (5.6)$$

The T_{prf} has been chosen as 1ms and 10 pulses are considered. Finally, the ten velocity image frames are averaged to obtain the CFM image.

We have used a low pass Gaussian filter to smoothen the velocity image reducing the noise with a 5x5 kernel and standard deviation of unity. The Gaussian kernel has been computed as:

$$G(x, y) = \frac{1}{2\pi} e^{-\frac{Z(x^2 + y^2)}{2\sigma^2}} \quad (5.7)$$

Where x, y are the pixels position of the kernel. This kernel is moved through the original velocity image and convolved to have the smooth image.

The total time required for a velocity image (256 lines and 10 frames averaged) simulation is 14015 seconds (~4 hours) for 17570 scatterers using MATLAB 7.8.0 in a computer with Intel Core-i3 3.3GHz processor, 4 GB RAM and Windows-7 64 bit operating system.

5.5 Summary

This chapter has discussed about computational fluid dynamics (CFD) simulation software ANSYS and ultrasound simulation software Field II with basics of transducer. In this work, blood flow is described by the incompressible Navier-Stokes equations and the simulation is carried out under steady conditions. The overall simulation methodology is described about the computational finite element model to simulate blood flow in carotid artery and their solution as well as the reconstruction of ultrasound color flow image (CFI) from FEM data.

CHAPTER VI

Result Analysis and Discussions

Chapter Outlines

- ❖ Introduction
- ❖ Analysis of CFD Simulated Images
- ❖ Analysis of Ultrasound Based Simulated Images
- ❖ Investigation on Viscosity Change Tracking Capability of Ultrasound Scanning
- ❖ Discussions

CHAPTER VI

Result Analysis and Discussions

6.1 Introduction

To achieve a more discernible representation of flow behavior the CFD and ultrasound based simulated images are examined in this chapter. The obtained CFD based flow images of different models under different conditions are presented first. These reference images are then used to compare with the simulated ultrasound based flow images to investigate its effectiveness for cardiovascular diseases diagnosis. Finally visual inspection and quantitative assessment has been done and discussed accordingly.

6.2 Analysis of CFD Simulated Images

The FEM model for normal and abnormal atherosclerosis cases for this study as described in the previous chapter has been solved using ANSYS Fluent. Steady state laminar flow is simulated in normal and atherosclerotic carotid artery to validate the coupling of the ultrasound and CFD setup. We have applied parabolic inlet boundary to mimic realistic blood flow as shown in Fig. 6.1.

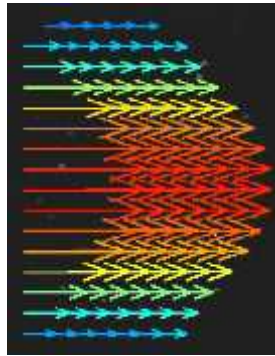


Figure 6.1 Parabolic velocity profile for inlet boundary condition

Figure 6.2 shows the normal and stenosed carotid artery bifurcation models with common carotid artery (CCA), internal carotid artery (ICA) and external carotid artery (ECA) and its x -directional computational velocity image with constant density of 1060 kg/m^3 and viscosity of

3.5 mPa-s. It has been observed that the parabolic velocity profile is visible in inlet boundary. The velocities in the normal carotid model are almost uniformly distributed. But the abnormal carotid models show the hemo-disturbance and blood velocity increased significantly in the plaque regions. Swirls have also been noticeable in the bifurcation. Most importantly, higher flow with velocity has been fairly observed in the narrower regions created by stenosis what usually happen in real cases.

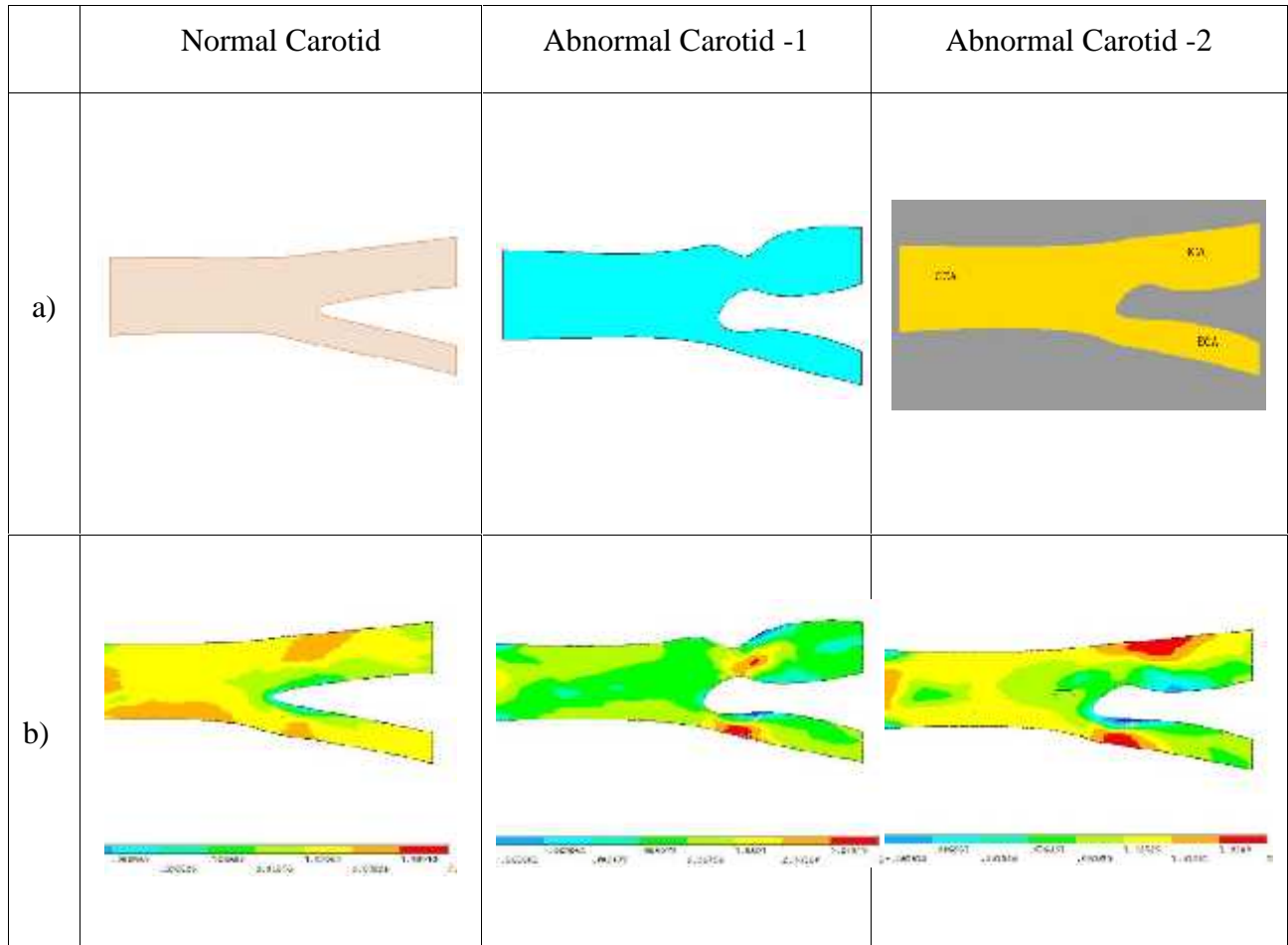


Figure 6.2 (a) Stenosed carotid artery model with bifurcation and (b) computed velocity image.

As blood viscosity is with atherosclerosis growth, viscosity related information can enhance the image quality of carotid atherosclerosis ultrasound image. Therefore, CFD images with varying viscosities has been computed to investigate the effect of viscosity as well as the

capability of ultrasound imaging to track this viscosity change. For this purpose, we use a fixed density of 1060 kg/m^3 and variable viscosity of $3.5 \text{ mPa}\cdot\text{s}$, $7 \text{ mPa}\cdot\text{s}$ and $10 \text{ mPa}\cdot\text{s}$ for the carotid atherosclerosis analysis to properly understand the growth of carotid atherosclerosis model-2. CFD simulation images for the 3 different blood viscosities are shown in Fig. 6.3. Though inlet velocity was 0.5 m/s , the maximum velocity reaches on about 2.5 m/s due to atherosclerosis stenosis. From the Fig. 6.3, it is observed that as the viscosity increases the magnitude of distributed velocities are reduced.

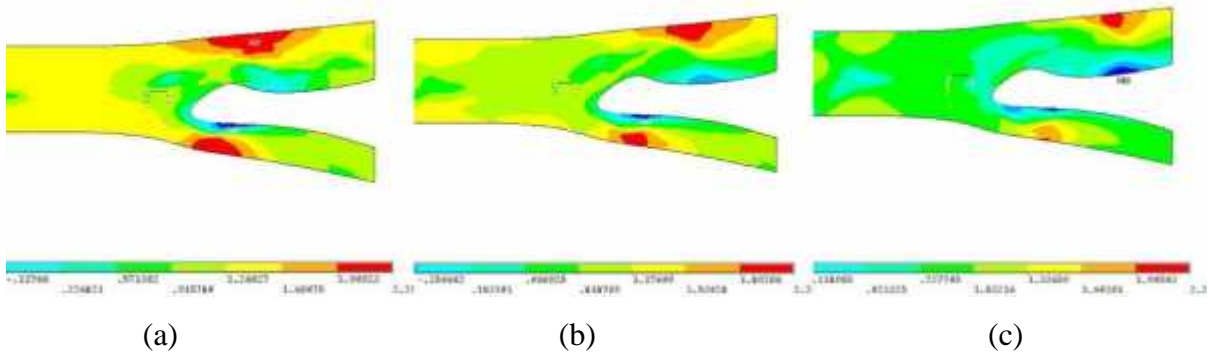


Figure 6.3 CFD simulation images for viscosities of (a) $3.5 \text{ mPa}\cdot\text{s}$, (b) $7 \text{ mPa}\cdot\text{s}$ and (c) $10 \text{ mPa}\cdot\text{s}$.

6.3 Analysis of Ultrasound Based Simulated Images

The contour plots of the estimated CFD velocities are a good reference to validate the performance of the ultrasound based flow imaging to fulfill the objectives of this simulation study. For ultrasound wave propagation simulation and radio frequency (RF) signal generation, we have used MATLAB based Field II program due to its accurate modeling of transducer properties, beam forming, wave propagation and interactions. We set a linear probe with 5 MHz center frequency and 100 MHz sampling rate was modeled. 256 RF lines were simulated using 128 transducer elements of which 64 active elements firing with focal length to cover the phantom. Hanning apodization is used to transmit and receive aperture. We have considered 10 time steps to generate RF signals for each frame using CFD data of 10 time steps. The velocity images are calculated using the autocorrelation based phase shift estimation algorithm as described in previous methodology chapter. These images can be compared with corresponding CFD simulation images. Ultrasound based color flow images

along with the CFD reference images are shown for the different models in Fig. 6.4. In the ultrasound color flow images (CFI), a parabolic velocity field can be observed which is in good agreement with that obtained from the CFD simulations with a slight underestimation of the velocities. For better analysis, the vector plot of CFD images are shown in Fig. 6.5. It has been observed that the flow direction deviated even in the opposite directions which indicate the negative velocity index in the contour plots of Fig. 6.4 in both CFD and ultrasound simulated images.

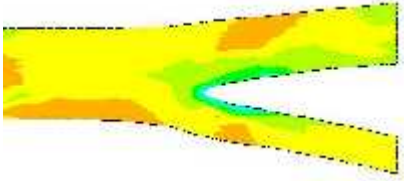
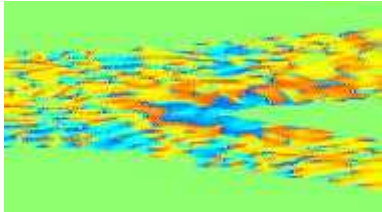
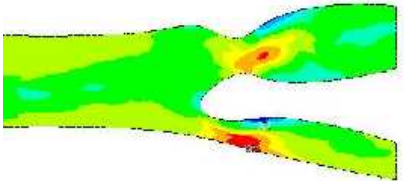
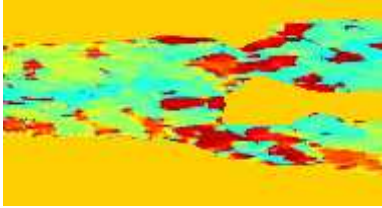
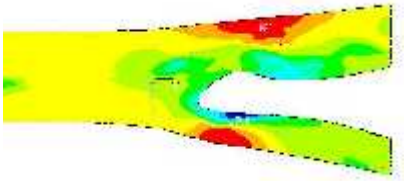
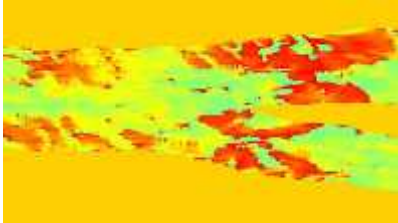
Model	CFD Simulated Flow Image	Ultrasound Simulated Flow Image
Normal Carotid Density: 1060 kg/m ³ Viscosity: 3.5 mPa-s		
Abnormal Carotid-1 Density: 1060 kg/m ³ Viscosity: 3.5 mPa-s		
Abnormal Carotid-2 Density: 1060 kg/m ³ Viscosity: 3.5 mPa-s		

Figure 6.4 Comparison of CFD computed and ultrasound simulated color flow velocity image for different blood flow models.

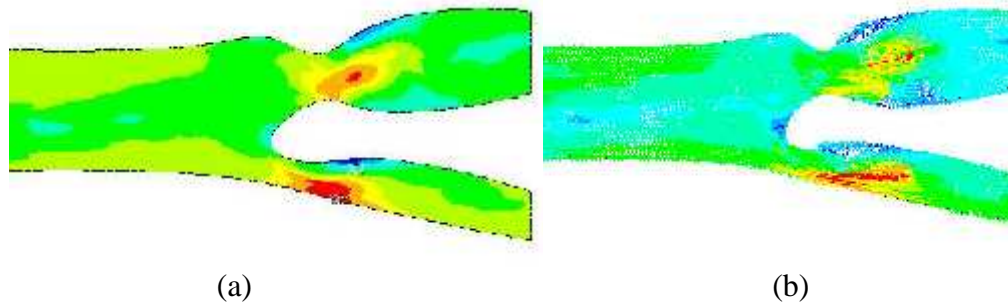


Figure 6.5 (a) Contour plot and (b) vector plot of velocity distribution for abnormal model-1.

6.4 Investigation on Viscosity Change Tracking Capability of Ultrasound Scanning

To investigate the capability of ultrasound imaging to track viscosity changes ultrasound simulated color flow images with varying viscosities has been compared with the reference CFD images as shown in Fig. 6.6. In the top CFD simulation image frame, where blood viscosity is 3.5 mPa-s (normal), the blood velocity is normal in the common carotid artery (CCA) and high velocity gradients are observed at the outer wall of the internal carotid artery (ICA) and external carotid artery (ECA) near the apex-induced separation due to atherosclerotic stenosis in the carotid bifurcated region that narrow the artery. The estimated velocity fields in the ultrasound color flow images show good agreement with the CFD results with a slight fluctuation.

Abnormal Carotid Model - 2	CFD Simulated Flow Image	Ultrasound Simulated Flow Image
Viscosity: 3.5 mPa-s		

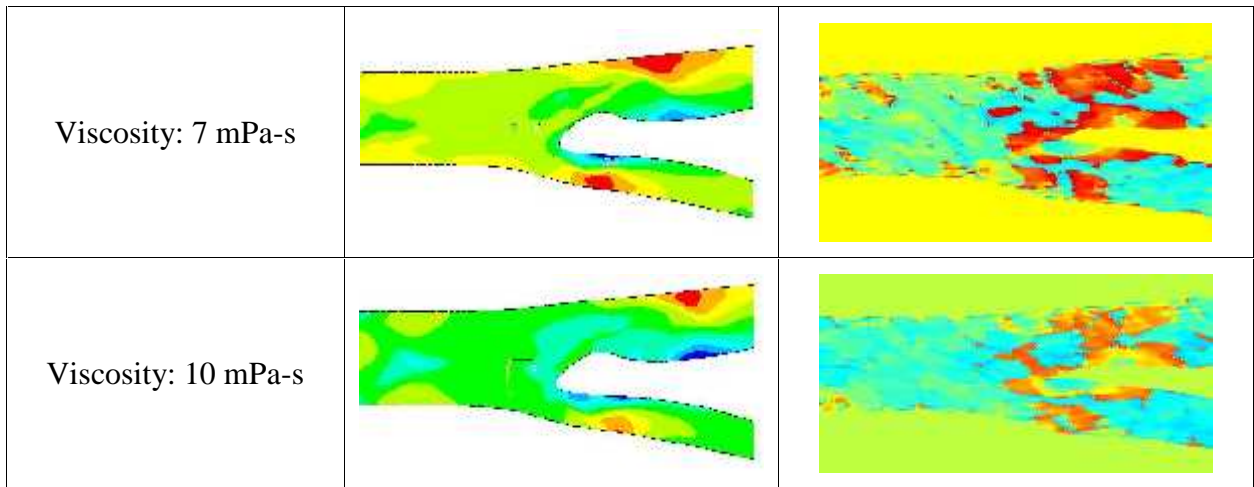


Figure 6.6 Comparison of CFD and ultrasound images considering viscosity changes.

In the middle simulation image frame, where blood viscosity is 7 mPa-s, the resistance of blood increases for increasing viscosity. As a result, blood velocity decreases in the CCA and arise complex flow pattern in the bifurcation region that is the cause of further growing of carotid atherosclerosis. The blood velocity also decreases in the ICA and ECA near the apex-induced separation. Insufficient blood might supply into the brain that is the indication of stroke. The estimated ultrasound color flow image shows slight fluctuation in compared to the CFD simulation image.

In the bottom CFD simulation image frame, where blood viscosity is 10 mPa-s, the resistance of blood highly increases for further increasing of viscosity. As a result, blood velocity more decreases in the CCA and a large zone of turbulence flow is present in the bifurcation which tends to grow carotid atherosclerosis and narrow the artery. The blood velocity more decreases in the ICA and ECA near the apex-induced separation and extremely less blood supplied that increases the risk of stroke. The estimated flow map in the ultrasound flow images show good agreement with the CFD results.

6.5 Discussions

It has been observed that higher flow with velocity is accomplished in the narrower regions created by stenosis in both CFD and ultrasound simulated images what are usually happened in real cases. However, there are some noises in the ultrasound simulated flow images even after low pass Gaussian filtering. These noises are come from ultrasound speckle and finite meshing and finite number of particles consideration. The magnitude of velocity vector sum considering all components in the atherosclerotic regions has been found 2-5 times faster than the inlet x-directional velocity.

Furthermore, as viscosity changes are associated with the growth of carotid atherosclerosis, tracking these changes and incorporation of this additional information can be useful to enhance the quality of ultrasound flow imaging. The hemodynamical disturbances in atherosclerotic carotid bifurcations for different level of blood viscosities are shown complex flow pattern during high degree of blood viscosity and significantly different from each other mainly due to different degrees of viscosities. From both CFD and ultrasound images, it is observed that the velocity images are different for different viscosity. As the viscosity increase with atherosclerosis growth, effective estimation of these velocity differences using ultrasound technique might provide additional information to enhance the quality of color flow image.

Table 6.1 Variation of blood velocity due to different stenosis

Models	ICA mean velocity (cm/sec)	ICA/CCA velocity ratio	Degree of Stenosis
Normal Carotid	116 (< 125)	1.2 < 2.0	Normal
Abnormal Carotid-1	333 (> 230)	4.7 (> 4.0)	Severe
Abnormal Carotid-2 Viscosity: 3.5 mPa-s	229 (125~230)	2.5(2.0~4.0)	Moderate
Abnormal Carotid-2 Viscosity: 7 mPa-s	210(125~230)	3(2.0~4.0)	Moderate
Abnormal Carotid-2 Viscosity: 10 mPa-s	190 (125~230)	3.2(2.0~4.0)	Moderate

The atherosclerosis stages of the models can be determined using the CFD data. Table 6.1 shows the mean velocity in the plaque regions of abnormal carotid models with their atherosclerosis stages. Depending on the mean velocity at ICA region of interests and the ICA/CCA velocity, the abnormal carotid model-1 shows the stenosis in severe level. The abnormal carotid model-2 for different viscosities are in moderate stages, but as the viscosity increases the ICA/CCA velocity ratios are increasing towards severe stage.

These findings of this study can enhance the potentiality of ultrasound based flow imaging in real time with its inherent fast scanning capability.

CHAPTER VII

Conclusions

Chapter Outlines

- ❖ Outcomes
- ❖ Contributions in this Research
- ❖ Limitations and Future Perspectives

CHAPTER VII

Conclusions

7.1 Outcomes

In this thesis work, the flow characteristics in different carotid atherosclerosis models have been analyzed using CFD and consequently simulated ultrasound color flow image have been tested and investigated. At first, the flow characteristic in the normal carotid artery has been observed. Then, the flow characteristics in abnormal carotid atherosclerosis bifurcations models have been investigated considering different realistic cases. The ultrasound simulated flow characteristics have been compared with CFD flow behavior and found a good agreement between them. It was perceived that the blood flow velocity increase noticeably in carotid atherosclerotic growths of abnormal carotid artery whereas blood velocity is almost uniform in the normal carotid artery. Furthermore, the models have been examined with varying viscosity as elevated viscosity is associated with atherosclerosis growth. It can be mentioned that viscosity effect investigation was a major emphasis of this study. The hemodynamical disturbances in atherosclerotic carotid bifurcations for different level of blood viscosities are shown more complex flow pattern during higher degree of blood viscosity and different from each other. In this study, it has been tested that ultrasound autocorrelation based flow imaging can track this viscosity induced differences. Therefore, an important finding of this study is viscosity induced contrast is not negligible and more importantly, it is detectable from multiple steps ultrasound flow images. As the conventional ultrasound flow imaging does not consider viscosity changes effect, the result analysis of this study suggests that incorporation of the viscosity changes contrast might enhance the quality of ultrasound flow image for carotid atherosclerosis diagnosis. We think the outcomes of this thesis work might be helpful to diagnosis the present conditions and predict the future progressions of carotid atherosclerosis disease to minimize the risk of brain stroke.

7.2 Contributions in this Research

A framework is presented that couples CFD and ultrasound simulations and allows generation of ultrasound signals resulting from realistic flow patterns in complex vessel geometries. The carotid atherosclerosis blood flow models for different realistic cases have been developed and studied using nonlinear Navier-Stokes equation based hemodynamic analysis concept. We have applied computational fluid dynamics and finite element analysis to solve the models. We have been done an effective CFD model to obtain a better understanding of diagnostic and functional aspects of the blood flow. The computed blood flow data are then used as synthetic phantom to generate ultrasound RF signals and flow images. The blood has been modeled as a collection of point scatterers moving with velocities given by the CFD velocity field, and the Field II simulation package is used to generate the backscattered ultrasound signals. Development of realistic models for CFD and synthetic phantom with scatterers positions, design of effective transducer array, selection of optimum simulation settings, apodization, generation of quality RF signals have been done with care. Autocorrelation based phase shift has been estimated efficiently from the Hilbert transformed backscattered ultrasound signals. A filter has been designed for developing ultrasound velocity images from the phase shift information. We have compared CFD simulation images with the ultrasound color flow images for proper validation. Finally, viscosity change effect has been investigated in order to detect and analyze the usefulness of viscosity related contrast in the diagnosis of carotid atherosclerosis and its growth.

7.3 Limitations and Future Perspectives

Although some significant findings have been obtained in this thesis work, there are some limitations also. In this work, the artery wall is considered as rigid. But, the human carotid artery is elastic. Consideration of complex fluid solid interaction can prove more realistic analysis. Furthermore, in practice the blood flow in human body has systole and diastole phase, but diastole event is neglected in this work. We have also noticed that some fluctuations in ultrasound color flow image even after filtering. 2D flow images have been simulated in this study. Though 2D flow images satisfy the objectives of this study, 3D flow imaging can provide better visualization and investigation scopes.

The above-mentioned limitations are planned to overcome in our future studies. We will try to construct 3D flow images using more practical 3D geometry and flow characteristics considering fluid solid interaction. Development of relevant effective signal processing methods for noise free color flow images will be our concern also. Such attempts can provide more information in favor of this study.

References

- 1 K. Strong, C. Mathers and R. Bonita, 2007, "Preventing stroke: saving lives around the world", *Lancet Neurol* 6: 182-187.
- 2 P. Libby, 2002, "Inflammation in atherosclerosis", *Nature* 420:868-874.
- 3 American Heart Association. Heart disease and stroke statistics - 2010 update. Technical report, American Heart Association, 2010.
- 4 Bangladesh NCD Risk Factor Survey, 2010.
- 5 J. J. Chiu, and S. Chien, 2011, "Effects of disturbed flow on vascular endothelium: pathophysiological basis and clinical perspectives", *Physiol Rev* 2011, 91(1): 327-87.
- 6 R. Krams, J. J. Wentzel, J. A. Oomen, R. Vinke, J. C. Schuurbiens, and P. J. de Feyter, 1997, et al. "Evaluation of endothelial shear stress and 3D geometry as factors determining the development of atherosclerosis and remodeling in human coronary arteries in vivo. Combining 3D reconstruction from angiography and IVUS (ANGUS) with computational fluid dynamics", *Arterioscler Thromb VascBiol* 1997, 17(10): 2061-5.
- 7 C. Wang, B. M. Baker, C. S. Chen, and M. A. Schwartz, 2013, "Endothelial cell sensing of flow direction", *Arterioscler Thromb VascBiol* 2013, 33(9): 2130-6.
- 8 P. Larsen, Oct. 2012, "Earlier, More Accurate Prediction of Cardiovascular Event Risk". [Online]. Available: <http://ndnr.com/cardiopulmonarymedicine/blood-viscosity>.
- 9 G. Lowe, A. Rumley, J. Norrie, I. Ford, J. Shepherd, S. Cobbe, and P. Macfarlane, 2000, "Blood Rheology, Cardiovascular Risk Factors, and Cardiovascular Disease: The West of Scotland Coronary Prevention Study". *Journal of Thrombosis and Haemostasis*, vol. 84, pp. 553–558.
- 10 R. C. Becker, 1993, "The role of blood viscosity in the development and progression of coronary artery disease". *Cleve Clin J Med.*, vol. 60, pp. 353–358.
- 11 G. Marom, H. S. Kim, M. Rosenfeld, E. Raanani, and R. Haj-Ali, 2012, "Effect of asymmetry on hemodynamics in fluid-structure interaction model of congenital bicuspid aortic valves". In *Proc. of International Conference of the IEEE Engineering in Medicine and Biology Society (EMBC)*, pp. 637– 640.

- 12 A. Swillens, J. Kips, H. Torp, and P. Segers, 2009, "Ultrasound simulation of complex flow velocity fields based on computational fluid dynamics". *IEEE Transactions on Ultrasonics, Ferroelectrics, and Frequency Control*, vol. 56.
- 13 E.Y. Wong, J. S. Milner, M. L. Thorne, H. N. Nikolov, D. A. Steinman, R. N. Rankin, T. L. Poepping, and D. W. Holdsworth, 2008, "Doppler ultrasound and numerical analysis for the assessment of hemodynamic disturbances in ulcerated carotid arteries". In *Proc. of IEEE International Ultrasonics Symposium*.
- 14 R. M. Nerem, 1992, "Vascular fluid mechanics, the arterial wall, and atherosclerosis". *Journal of Biomechanical Engineering*, vol. 114, pp.274–282.
- 15 L. C. Sousa¹, C. F. Castro¹, C. C. António¹, F. Sousa, R. Santos, P. Castro, and E. Azevedo, 2013, "Stenosed carotid bifurcation: hemodynamics and wall shear stress". In *Proc. of 4th International Conference on Integrity, Reliability and Failure*.
- 16 A. M. Malek, S. L. Alper, and S. Izumo, 1999, "Hemodynamic shear stress and its role in atherosclerosis". *Journal of the American Medical Association*, vol. 282, pp. 2035–2041.
- 17 <http://hillviewprimary.edublogs.org/2013/10/03/year-5-science-systems-of-our-body/>
- 18 R. Ross, 1999, "Atherosclerosis: an inflammatory disease". *N. Engl. J. Med.*340: 115–26.
- 19 C. Weber, A. Zernecke, and P. Libby, 2008, "The multifaceted contributions of leukocyte subsets to atherosclerosis: lessons from mouse models". *Nat. Rev. Immunol.*8:802–15.
- 20 G. K. Hansson, and P. Libby, 2006, "The immune response in atherosclerosis: a double-edged sword". *Nat. Rev. Immunol.*6:508–19.
- 21 C. Napoli, F. P. D'Armiento, and F. P. Mancini, 1997, et al. "Fatty streak formation occurs in human fetal aortas and is greatly enhanced by maternal hypercholesterolemia: intimal accumulation of low density lipoprotein and its oxidation precede monocyte recruitment into early atherosclerotic lesions". *J Clin Invest*, 100: 2680-90.
- 22 H. C. Sary, A. B. Chandler, and S. Glagov, 1994, et al. "A definition of initial, fatty streak, and intermediate lesions of atherosclerosis: a report from the Committee on Vascular Lesions of the Council on Arteriosclerosis". *American Heart Association, Circulation*, 89: 2462-78.
- 23 N. Simionescu, E. Vasile, F. Lupu, G. Popescu, and M. Simionescu, 1986, "Prelesional events in atherogenesis: accumulation of extracellular cholesterol-rich liposomes in the arterial intima and cardiac valves of the hyperlipidemic rabbit". *Am J Pathol*, 123: 109-25.

- 24 M. Fisher, A. Martin, M. Cosgrove, and J. W. Norris, 1993, "The NASCET-ACAS plaque project. North American Symptomatic Carotid Endarterectomy Trial. Asymptomatic Carotid Atherosclerosis Study", *Stroke*, (12 Suppl):124-5, (discussion: 131-2).
- 25 R. Ross, and J. A. Glomset, 1973, "Atherosclerosis and the arterial smooth muscle cell: proliferation of smooth muscle is a key event in the genesis of the lesions of atherosclerosis". *Science*, 180:1332-9.
- 26 Idem., 1976, "The pathogenesis of atherosclerosis". *N Engl J Med*, 295: 369-77, 420-5.
- 27 R. Ross, 1986, "The pathogenesis of atherosclerosis: an update". *N Engl J Med*, 314: 488-500.
- 28 Idem., 1993, "The pathogenesis of atherosclerosis: a perspective for the 1990s". *Nature*, 362: 801-9.
- 29 R. Ross, 1981, "Atherosclerosis: a problem of the biology of arterial wall cells and their interactions with blood components". *Arteriosclerosis*, 1: 293-311.
- 30 S. Glagov, E. Weisenberg, C. K. Zarins, R. Stankunavicius, and G. J. Kolettis, 1987, "Compensatory enlargement of human atherosclerotic coronary arteries". *N Engl J Med*, 316:1371-5.
- 31 H. C. Stary, 1996, "The histological classification of atherosclerotic lesions in human coronary arteries". In: Fuster V, Ross R, Topol EJ, eds. "Atherosclerosis and coronary artery disease". Philadelphia: Lippincott-Raven, Vol. 1. :463-74.
- 32 L. Jonasson, J. Holm, O. Skalli, G. Bondjers, and G. K. Hansson, 1986, "Regional accumulations of T cells, macrophages, and smooth muscle cells in the human atherosclerotic plaque". *Arteriosclerosis*, 6: 131-8.
- 33 A. C. van der Wal, P. K. Das, D. Bentz van de Berg, C. M. van der Loos, and A. E. Becker, 1989, "Atherosclerotic lesions in humans: in situ immunophenotypic analysis suggesting an immune mediated response". *Lab Invest*, 61:166-70.
- 34 P. Libby, and R. Ross, 1996, "Cytokines and growth regulatory molecules". In: V. Fuster, R. Ross, E. J. Topol, eds. "Atherosclerosis and coronary artery disease". Philadelphia: Lippincott-Raven, Vol. 1. :585-94.
- 35 E. W. Raines, M. E. Rosenfeld, and R. Ross, 1996, "The role of macrophages". In: V. Fuster, R. Ross, E. J. Topol, eds. "Atherosclerosis and coronary artery disease". Philadelphia: Lippincott-Raven, Vol. 1. : 539-55.

- 36 E. Falk, P. K. Shah, and V. Fuster, 1996, "Pathogenesis of plaque disruption". In: V. Fuster, R. Ross, E. J. Topol, eds. "Atherosclerosis and coronary artery disease". Philadelphia: Lippincott-Raven, Vol.2. : 492-510.
- 37 <https://iame.com/online-courses/ultrasound-vascular/carotid-duplex-examination-for-rt>
- 38 E. Ralph, Holsworth, D. O. Jr., and J. V. Wright, 2012, "Blood Viscosity: The Unifying Parameter In Cardiovascular Disease Risk", MD - Vol. 13, No. 1.
- 39 R. Ross, 1999, "Atherosclerosis: an inflammatory disease". N Engl J Med, 340: 115-26.
- 40 P. Libby, P. M. Ridker, and A. Maseri, 2002, "Inflammation and atherosclerosis". Circulation, 105: 1135-43.
- 41 P. Libby, and M. Ridker, 1999, "Novel inflammatory markers of coronary risk: theory versus practice". Circulation, 100: 148-50.
- 42 P. M. Ridker, N. Rifai, and M. J. Stampfer, 2000, "Plasma concentration of interleukin- 6 and the risk of future myocardial infarction among apparently healthy men". Circulation, 342: 836-43.
- 43 X. Weng, G. Cloutier, R. Beaulieu, and G. O. Roederer, 1996, "Influence of acute phase proteins on erythrocyte aggregation". Am J Physiol, 271: H2346-52.
- 44 H. Schmid-Schonbein, H. Malotta, and F. Striesow, 1990, "Erythrocyte aggregation: causes, consequences and methods of assessment". Tijdschr NVKC, 15:88-97.
- 45 R. Ben Ami, G. Barshtein, D. Zeltser, Y. Goldberg, I. Shapira, and A. Roth, 2001, et al. "Parameters of red blood cell aggregation as correlates of the inflammatory state". Am J Physiol Heart CircPhysiol, 280: H1982-H8.
- 46 M. Woodward, A. Rumley, Tunstall-Pedoe, and G. D. O. Lowe, 1999, "Associations of blood rheology and interleukin-6 with cardiovascular risk factors and prevalent cardiovascular disease". Br. J. Haemat, 104: 246-57.
- 47 F. J. Neumann, H. A. Katus, and E. Hoberg, 1991, "Increased plasma viscosity and erythrocyte aggregation: indicators of an unfavourable clinical outcome in patients with unstable angina pectoris". Br Heart J, 66: 425-30.
- 48 J. W. G. Yarnell, I. A. Baker, P. M. Sweetnam, D. Bainton, J. R. O'Brien, and P. J. Whitehead, 1991, et al. "Fibrinogen, viscosity, and white blood cell count are major risk factors for ischemic heart disease". "The Caerphilly and Speedwell Collaborative Heart Disease Studies". Circulation, 83: 836-44.

- 49 G. D. Sloop, 1996, "A unifying theory of atherogenesis". *Med Hypotheses*, 47: 321-5.
- 50 C. G. Gustavsson, S. Persson, B. O. Thorvinger, and P. Hedner, 1997, "Association between pre-PTCA blood haemoglobin concentration and the risk of symptomatic restenosis after successful PTCA of primary coronary stenoses". *J Cardiovasc Risk*, 4: 37-40.
- 51 G. D. O. Lowe, J. C. Barbenel, and C. D. Forbes, 1981, "Clinical aspects of blood viscosity and cell deformability". Berlin Heidelberg New York, Springer Verlag: 67-79.
- 52 D. A. McDonald, "Blood flow in arteries, UK: Edward Arnold, 5th edn. London.
- 53 S. Oka., "Cardiovascular hemorheology", Cambridge, UK: Cambridge University Press.
- 54 S. Chien, S. Usami, H. M. Taylor, J. L. Lundberg and M. I. Gregersen, 1966, "Effects of hematocrit and plasma proteins on human blood rheology at low shear rates", *J. Appl. Physiol.*, 21: 81-87.
- 55 S. Chien, 1970, "Shear dependence of effective cell volume as a determinant of blood viscosity", *Science*, Volume 169, Issue 3934, 977-979.
- 56 A. C. Guyton, 1961, "Textbook of medical physiology". *The American Journal of the Medical Sciences*, vol. 242, no. 2, p. 136.
- 57 J. A. Sethian, 1993, "Computational fluid dynamics, In: From Desktop to Teraflop: Exploiting the US Lead in High Performance Computing". NSF Publications, National Science Foundation, Washington DC, USA.
- 58 J. N. Reddy, 2005, "An Introduction to the Finite Element Method", McGraw-Hill, Third ed., ISBN 9780071267618.
- 59 I. Edler, and K. Lindstrom, 2004, "The history of echocardiography", *Ultrasound Med Biol.* 30: 1565–1644.
- 60 S. Satomura., 1957, "Ultrasonic Doppler method for the inspection of cardiac functions". *J. Acoust. Soc. Am.*, 29: 1181–1185.
- 61 K. Namekawa, C. Kasai, M. Tsukamoto, and A. Koyano, 1982, "Real time blood flow imaging system utilizing autocorrelation techniques". In *Ultrasound '82* (eds. R. A. Lerski, P. Morley), pp. 203–208, New York, NY: Pergamon Press.
- 62 C. Kasai, K. Namekawa, A. Koyano, and R. Omoto, 1985, "Real-time two-dimensional blood flow imaging using an autocorrelation technique". *IEEE Trans. Son. Ultrason.* 32, 458–463.

- 63 C. M. Otto, 2000, "Principles of echocardiographic image acquisition and Doppler analysis". In: Textbook of Clinical Ecocardiography, 2nd ed., Philadelphia, PA: W.B Saunders, 2000: 1–29.
- 64 A. E. Weyman, 1994, "Physical principles of ultrasound, In: A. E. Weyman, ed. Principles and Practice of Echocardiography", 2nd ed. Media, PA: Williams & Wilkins; 1994:3–28.
- 65 J. P. Lawrence, 2007, "Physics and instrumentation of ultrasound". Crit Care Med., 35: S314–S322.
- 66 P. A. Peronneau and F. Leger, 1969, "Doppler ultrasonic pulsed blood flowmeter". In Proc. 8th Int. Conf. Med. Biol. Eng., pages 10–11.
- 67 V. W. S. Chan, 2009, "Ultrasound Imaging for Regional Anesthesia". 2nd ed. Toronto, ON: Toronto Printing Company.
- 68 J. A. Jensen., 1996, "Estimation of Blood Velocities Using Ultrasound: A Signal Processing Approach". Cambridge University Press, New York.
- 69 C. Kasai, K. Namekawa, A. Koyano, and R. Omoto., 1985, "Real-time two-dimensional blood flow imaging using an autocorrelation technique". IEEE Trans. Sonics Ultrason., vol. SU-32, pp. 458-464.
- 70 B. A. J. Angelsen and K. Kristoffersen, 1979, "On ultrasonic MTI measurement of velocity profiles in blood flow", IEEE Trans. Biomed. Eng., vol. BME-26, pp. 665-671.
- 71 A. Papoulis, 1965, "Probability, Random Variables and Stochastic Processes". New York: McGraw-Hill.
- 72 H. Torp, K. Kristoffersen, and B. Angelsen, 1994 "Autocorrelation technique in color flow imaging, signal model and statistical properties of the autocorrelation estimates". IEEE Trans. Ultrason., Ferroelect., Freq. Contr., vol. 41, pp. 604-612.
- 73 K. W. Ferrara, V. R. Algaz, 1992, et al., "The effect of frequency dependent scattering and attenuation on the estimation of blood velocity using ultrasound". IEEE Trans. Ultrason., Ferroelect., Freq. Contr., vol. 39, pp. 754-767.
- 74 C. Kasai, K. Namekawa, A. Koyano, and R. Omoto., 1985, "Real-time two-dimensional blood flow imaging using an autocorrelation technique". IEEE Trans. Sonics Ultrason., vol. SU-32, pp. 458-464.
- 75 T. Loupas, J. T. Powers, and R. W. Gill, 1995, "An axial velocity estimator for ultrasound blood flow imaging, based on a full evaluation of the Doppler equation by means of a two-

- dimensional autocorrelation approach". IEEE Trans. Ultrason., Ferroelect., Freq. Contr., vol. 42, pp. 672-688.
- 76 H. Torp and K. Kristoffersen, 1996, "Method for calculation of blood velocity and blood velocity spread from multi gated Doppler signal" U.S. Patent No. 5.560.363.
- 77 W. D. Barber, J. W. Eberhard, and S. G. Karr, 1985, "A new time domain technique for velocity measurements using Doppler ultrasound". IEEE Trans. Biomed. Eng. 32: 213-29.
- 78 E. Nguyen-Khac, and D. Capron, 2006, "Noninvasive diagnosis of liver fibrosis by ultrasonic transient elastography (Fibroscan)". European Journal of Gastroenterology & Hepatology 18: 1321-1325.
- 79 M. Berrutti, A. Ciancio, and A. Smedile et al., 2007, "Assessment of liver fibrosis in the clinical setting: something is changing?", Minerva Gastroenterologicae Dietologica 53: 111-114.
- 80 R. De Franchis, and A. Dell'Era, 2007, "Non-invasive diagnosis of cirrhosis and the natural history of its complications". Best Practice & Research in Clinical Gastroenterology 21: 3-18.
- 81 J. A. Jensen, 1993, "Implementation of ultrasound time-domain cross-correlation blood velocity estimators". IEEE Trans. Biomed. Eng., 40:468-474.
- 82 <http://www.healthylifescreeing.com/carotid.html>
- 83 J. Biasetti, F. Hussain and T. C. Gasser., 2011, "Blood flow and coherent vortices in the normal and aneurysmatic aortas: a fluid dynamical approach to intra-luminal thrombus formation". J. R. Soc. Interface, 8: 1449-1461.
- 84 J. A. Jensen, 1991, "A model for the propagation and scattering of ultrasound in tissue". Journal of the Acoustical Society of America, vol. 89, pp. 182-190.
- 85 J. A. Jensen, 1996, "Field: A program for simulating ultrasound systems". Medical & Biological Engineering & Computing, vol. 34, pp. 351-353.
- 86 M. Schlaikjer, S. Torp-Pedersen, and J. A. Jensen, 2003, "Simulation of RF data with tissue motion for optimizing stationary echo canceling filters", Ultrasonics, vol. 41, pp. 415-419.
- 87 G. E. Tupholme, 1969, "Generation of acoustic pulses by baffled plane pistons", Mathematika 16, pp. 209-224.

- 88 P. R. Stepanishen, 1971A, “The time-dependent force and radiation impedance on a piston in a rigid infinite planar baffle”, J. Acoust. Soc. Am. 49 (3), pp. 841-849.
- 89 P. R. Stepanishen, 1971B, “Transient radiation from pistons in an infinite planar baffle”, J. Acoust. Soc. Am. 49, pp. 1627-1638.
- 90 P. R. Stepanishen, 1981, “Pulsed transmit/receive response of ultrasonic piezoelectric transducers”, J. Acoust. Soc. Am. 69, pp. 1815-1827.
- 91 J. A. Jensen and N. B. Svendsen, 1992, “Calculation of pressure fields from arbitrarily shaped, apodized, and excited ultrasound transducers”. IEEE Trans. Ultrason., Ferroelec., Freq. Contr., 39, pp. 262-267.
- 92 J. A. Jensen, 2001, “Speed-accuracy trade-offs in computing spatial impulse responses for simulating medical ultrasound imaging”, J. Comput. Acoust., vol. 9, pp. 731–744.

List of Publication

1. Dabasish Kumar Saha and A. B. M. Aowlad Hossain, “A Simulation Study on Viscosity Change Effects in Ultrasound Based Carotid Atherosclerosis Diagnosis,” *Proc. of 3rd International Conference on Advances in Electrical Engineering (ICAEE)*, Dhaka, Bangladesh, 17-19 December 2015. (Available in *IEEE xplore*)